Earth-Science Reviews 197 (2019) 102918

Contents lists available at ScienceDirect

Earth-Science Reviews

journal homepage: www.elsevier.com/locate/earscirev

Congo River sand and the equatorial quartz factory

Eduardo Garzanti[a,*], Pieter Vermeesch[b], Giovanni Vezzoli[a], Sergio Andò[a], Eleonora Botti[a], Mara Limonta[a], Pedro Dinis[c], Annette Hahn[d], Daniel Baudet[e], Johan De Grave[f], Nicole Kitambala Yaya[g]

[a] Laboratory for Provenance Studies, Department of Earth and Environmental Sciences, University of Milano-Bicocca, 20126 Milano, Italy
[b] London Geochronology Centre, Department of Earth Sciences, University College London, London, WC1E 6BT, UK
[c] Department of Earth Sciences, MARE – Marine and Environmental Sciences Centre, University of Coimbra, Portugal
[d] MARUM Center for Marine Environmental Sciences, University of Bremen, Bremen, Germany
[e] Geodynamics & Mineral Resources, Royal Museum for Central Africa (RMCA), Leuvensesteenweg 13, 3080 Tervuren, Belgium
[f] Department of Geology and Soil Science (WE13), MINPET, Ghent University, Krijgslaan 281/S8, WE13, B-9000 Gent, Belgium
[g] CRGM Centre de Recherches Géologiques et Minières, 44, Av. de la Démocratie, Kinshasa-Gombe, Democratic Republic of Congo

ARTICLE INFO

Keywords:
Provenance analysis
Equatorial weathering
U-Pb zircon geochronology
Zircon weatherability
Calcite dissolution
Chemical indicators of weathering and recycling
First-cycle versus polycyclic quartzarenites
Volcanic provenance of offshore muds

ABSTRACT

A never solved problem in sedimentary petrology is the origin of sandstone consisting exclusively of quartz and most durable heavy minerals. The Congo River offers an excellent test case to investigate under which tectonic, geomorphological, climatic, and geochemical conditions pure quartzose sand is generated today. In both upper and lowermost parts of the catchment, tributaries contain significant amounts of feldspars, rock fragments, or moderately stable heavy minerals pointing at the central basin as the main location of the "quartz factory". In Congo sand, quartz is enriched relatively to all other minerals including zircon, as indicated by Si/Zr ratios much higher than in the upper continental crust. Selective elimination of old zircons that accumulated radiation damage through time is suggested by low percentages of grains yielding Archean U—Pb ages despite the basin being surrounded by Archean cratonic blocks. Intense weathering is documented by the lack of carbonate grains in sand and by dominant kaolinite and geochemical signatures in mud. In sand, composed almost entirely of SiO_2, the weathering effect is masked by massive addition of quartz grains recycled during multiple events of basin inversion since the Proterozoic.

Changes in mineralogical, geochemical, and geochronological signatures across Bas-Congo concur to suggest that approximately 10% of the sand supplied to the Atlantic Ocean is generated by rapid fluvial incision into the recently uplifted Atlantic Rise. The Congo River connects with a huge canyon ~30 km upstream of the mouth, and pure quartzose sand is thus funnelled directly toward the deep-sea to feed a huge turbidite fan. Offshore sediments on both sides of the canyon are not derived from the Congo River. They reflect mixed provenance, including illite-rich dust wind-blown from the arid Sahel and augite, hypersthene, and smectite ejected from volcanic centres probably situated along the Cameroon Line in the north.

Because mixing of detritus from diverse sources and supply of polycyclic grains almost invariably occurs in the terminal lowland tract of a sediment-routing-system, no ancient sandstone can be safely considered as entirely first-cycle. Moreover, the abundance of pure quartzarenite in the rock record can hardly be explained by chemical weathering or physical recycling alone. The final cleansing of minerals other than quartz, zircon, tourmaline, and rutile requires one or more cycles of chemical dissolution during diagenesis, which operates at higher temperatures and over longer periods than weathering at the Earth's surface.

* Corresponding author.
E-mail addresses: eduardo.garzanti@unimib.it (E. Garzanti), p.vermeesch@ucl.ac.uk (P. Vermeesch), giovanni.vezzoli@unimib.it (G. Vezzoli), sergio.ando@unimib.it (S. Andò), e.botti4@campus.unimib.it (E. Botti), mara.limonta@unimib.it (M. Limonta), pdinis@dct.uc.pt (P. Dinis), ahahn@marum.de (A. Hahn), daniel.baudet@africamuseum.be (D. Baudet), johan.degrave@ugent.be (J. De Grave).

https://doi.org/10.1016/j.earscirev.2019.102918
Received 30 March 2019; Received in revised form 19 July 2019; Accepted 28 July 2019
Available online 30 July 2019
0012-8252/

> "… *a mighty big river resembling an immense snake uncoiled, with its head in the sea, its body at rest curving afar over a vast country, and its tail lost in the depths of the land.*"
>
> Joseph Conrad – Heart of Darkness

1. Introduction

The large-scale production of pure quartzose sand stands as a long-debated, particularly thorny issue in sedimentary petrology (Krynine, 1941; Pettijohn et al., 1972: pp. 223–227; Suttner et al., 1981; Chandler, 1988; Johnsson et al., 1988; Dott, 2003; Mehring and McBride, 2007; Basu, 2017). Can prolonged weathering promoted by extreme hot-humid climatic conditions or in situ leaching in soils by infiltrating rainwater rich in humic acids be efficient enough to eliminate all but the few most durable species of detrital minerals (van Loon, 2009)? Or should the generation of residual sand composed only of quartz, zircon, tourmaline, and rutile necessarily imply the effect of chemical dissolution accumulated through more than a single sedimentary cycle, considering that the time and temperature available for chemical reactions are much longer and higher during burial diagenesis than at the Earth's surface (McBride, 1985)? If entirely first-cycle pure quartzose sand does exist, then what climatic (e.g., temperature, precipitation), geomorphological (e.g., topography, vegetation, soil processes, groundwater level), and chemical conditions (e.g., type and concentration of dissolved ions in reacting fluids, *pH*, *Eh*) are required for its generation (Basu, 1985; Johnsson, 1993)? To shed new light on these challenging questions we moved to hot and hyper-humid Congo in cratonic equatorial Africa, a particularly well suited environmental setting for a "quartz factory".

The Congo is the largest river on Earth that carries pure quartzose sand to the world's oceans (Fig. 1). Other big rivers supplying pure quartzose sand to the Atlantic Ocean include the Paranà and Uruguay in South America, whereas Orinoco sand is quartzose with a few sedimentary and low-rank metasedimentary lithics derived from the northern Andes, and Amazon sand is feldspatho-litho-quartzose (Fig. 6 in Garzanti, 2019). Other large African rivers do carry pure quartzose sand but only in the continental interiors, including the White Nile, the Zambezi upstream of Victoria Falls, and the Okavango draining into the Kalahari Desert of central Botswana (Garzanti et al., 2014a, 2015).

2. The Congo River

The huge catchment of the 4700 km-long Congo River (basin area 3.7 10^6 km^2, 12% of Africa, ~2.2% of the Earth's land surface) is the second-longest in Africa and ninth-longest in the world. The drainage basin, straddling the Equator from ~13°S to ~9°N, is delimited by the late Mesozoic Central African rift system to the north, by the mid-Cenozoic East African rift system to the east, and by the Kalahari Plateau to the south (Leturmy et al., 2003). The two major tributaries are the Kasai (Cassai) from the south and the Ubangui (Oubangui, Ubangi) from the north. The major headwater branch is the Lualaba, and the longest one the Chambeshi. The Lukuga River is the outlet of Lake Tanganyika, whereas major rivers flowing into Lake Tanganyika include the Rusizi in Burundi and the Malagarasi in Tanzania (Fig. 2).

The central part of the basin (*cuvette centrale*), a wide depression accounting for ~30% of the entire catchment, is characterized by equatorial climate with 2.0–2.3 m of annual rainfall (Alsdorf et al., 2016). In these lowlands, covered by loose clay and sand, the Congo River has very low slope and flow velocity (0.3–0.6 m/s). A permanently or temporarily flooded rain forest, extending toward rift highlands in the east where precipitation reaches 2.5 m/a, has been sustained since it replaced savannahs after the dry time of the Last Glacial Maximum (Runge, 2007). Transition to humid tropical climate with

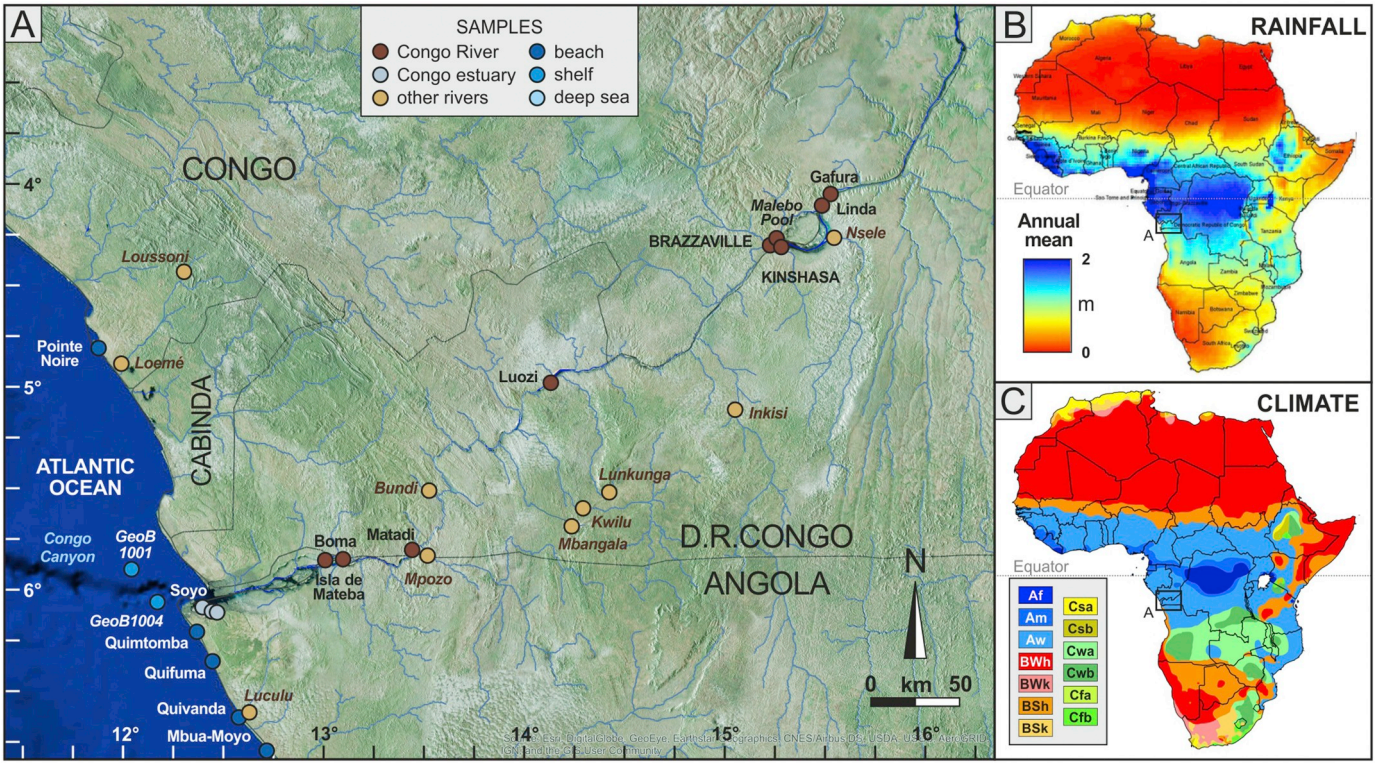

Fig. 1. The Congo River in Bas-Congo (now Kongo Central province). (A) Location map with sampling sites (DEM files sourced from USGS www.usgs.gov/foia/index.htm). The steep juvenile tract of the river between Kinshasa and Matadi includes the Inga Falls, the largest rapids of the world where water rushes at 14 m/s and waves reach 12 m (Figs. 3 and 4). (B) Rainfall data after Masih et al. (2014). (C) Climate classification after Kottek et al. (2006): A = equatorial (f = fully humid; m = monsoonal; w = winter dry); B = arid (W = desert; S = steppe; h = hot; k = cold); C = warm temperate (f = fully humid; s = summer dry; w = winter dry; a = hot summer; b = warm summer).

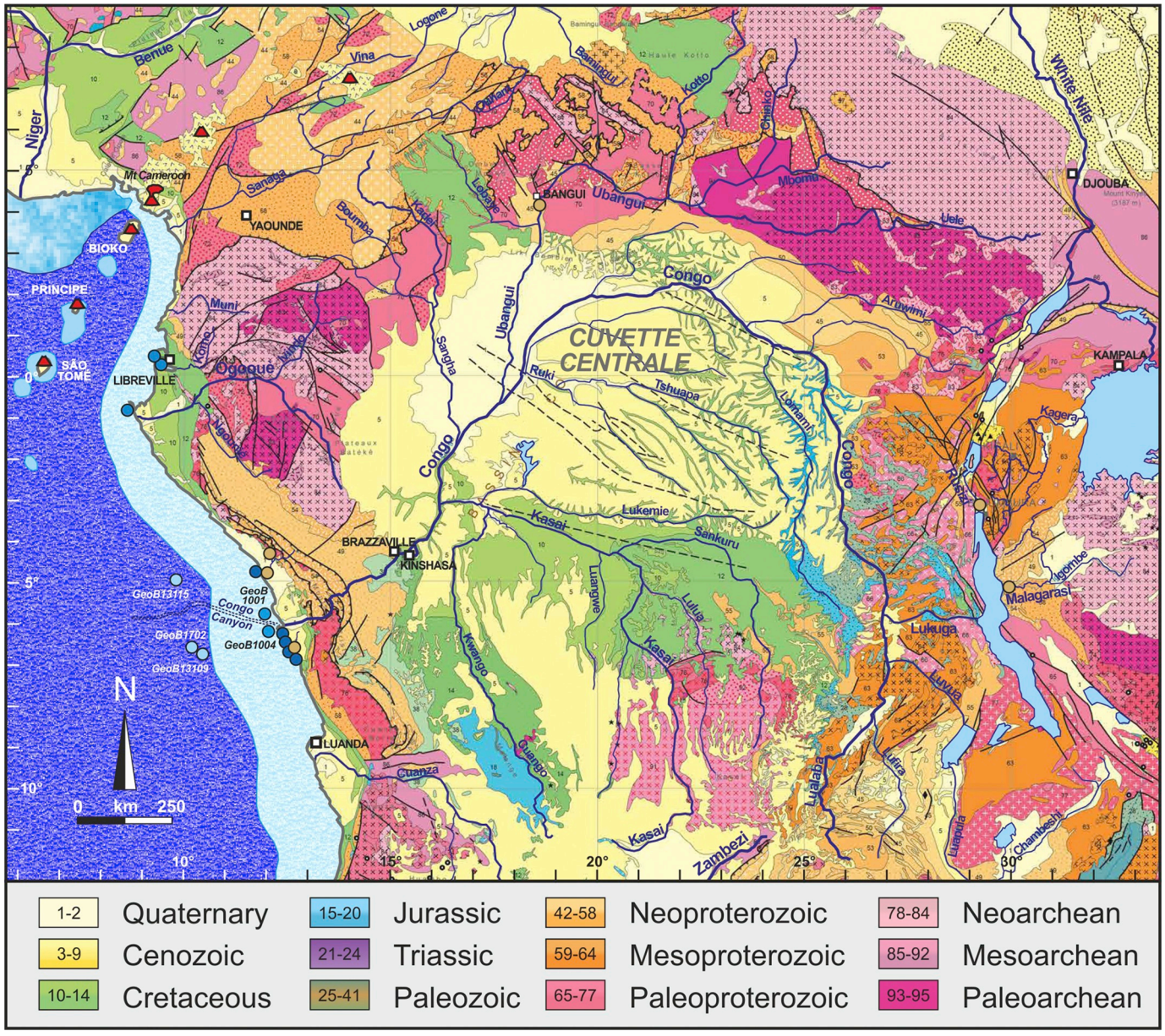

Fig. 2. Geological map of the Congo catchment and adjacent regions (CGMW-BRGM, 2016). Location of coastal and offshore samples, as well as river samples collected in coastal areas and outside of Fig. 1 are shown. Congo Canyon after Wenau et al. (2015).

annual precipitation decreasing to 1.4–1.8 m occurs both northwards and southwards, where shield plateaus are covered by shrub and tree savannah. The northern divide of the basin drained by Ubangui tributaries is semiarid, whereas in the south alternating wet and dry seasons with notably lower temperatures characterize the Angolan and Shaba highlands, covered by open savannah woodland or dry deciduous forest interspersed with grassland and wetland.

The northward direction of major tributaries sourced in Angolan and Shaba highlands and provenance analysis of Jurassic-Cretaceous sandstones has led to think that the paleo-Congo river originally flowed from south to north (Agyemang et al., 2016), possibly as far as Lake Chad (Runge, 2007: p. 302). Alternative hypotheses are that in the Late Cretaceous to Paleogene the *cuvette centrale* drained eastwards entering the Indian Ocean at the present Rufiji Delta in Tanzania (Stankiewicz and de Wit, 2006), or westwards entering the Atlantic Ocean at the present Ogooué Delta in Gabon (Karner and Driscoll, 1999: p. 29). A major drainage change in Oligo-Miocene times was induced by southward propagation of the East African rift and associated rift-shoulder uplift and subsidence of the *cuvette centrale* (Guillocheau et al., 2018). There is no consensus whether the youthful terminal tract of the river resulted from capture by a short headward-eroding coastal stream (Goudie, 2005) or was antecedent relative to recent uplift (Flügel et al., 2015), and whether the Congo River outlet has remained fixed since the Late Cretaceous (Anka et al., 2010; Linol et al., 2015a) or was established in the Oligocene (Karner and Driscoll, 1999; Savoye et al., 2000), middle/late Miocene (Uenzelmann-Neben, 1998), or only very recently in the early Pleistocene (Peters and O'Brien, 2001; Giresse, 2005).

2.1. The lower course, the canyon, and the fan

Just upstream of Brazzaville and Kinshasa, the capitals of the Republic of Congo and of the Democratic Republic of Congo, lies the Malebo (Stanley) Pool, where the river widens to 20–25 km, it is only 3–10 m deep, and sand bars emerge during low flow. Between Kinshasa and the Atlantic Ocean, the channel drops by ~270 m over a distance of ~500 km. In this steep juvenile tract known as Livingstone Falls

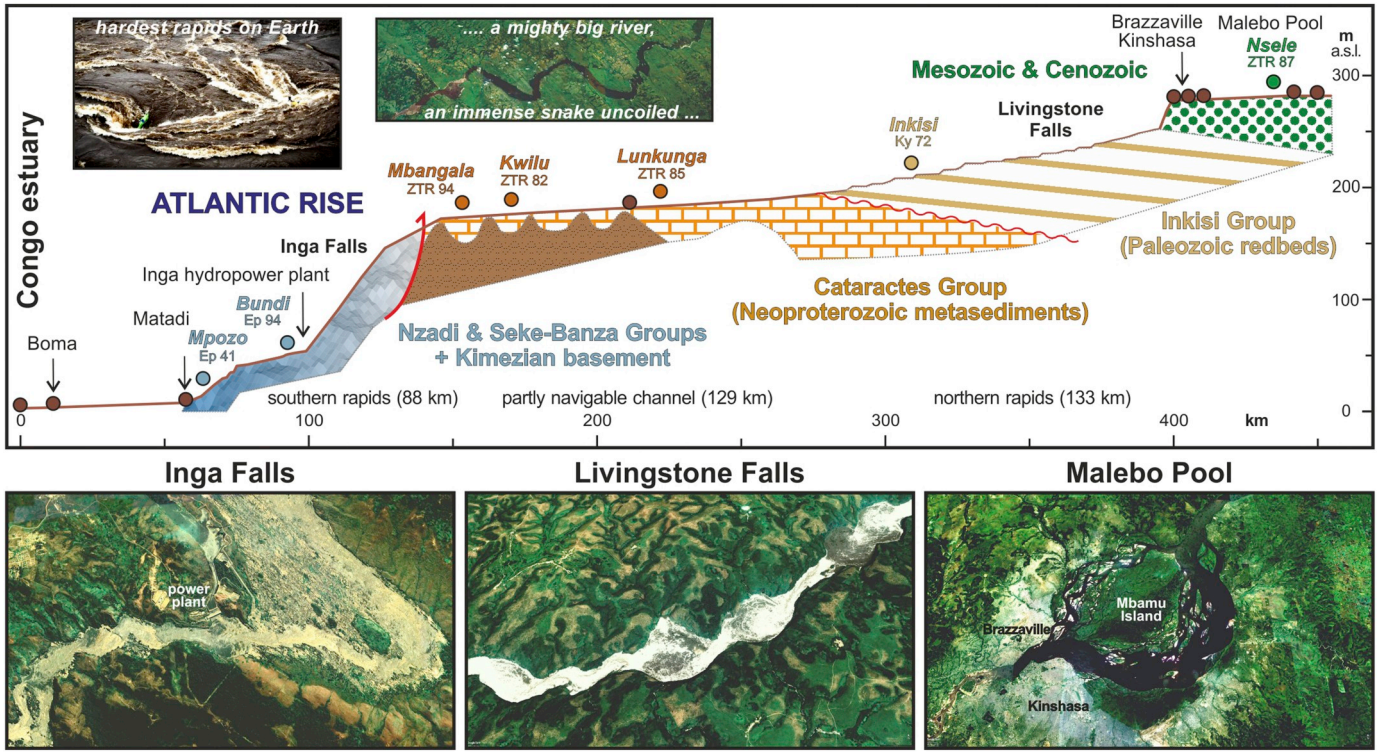

Fig. 3. Longitudinal profile of the trunk-river in Bas-Congo (modified after fig. 14.3 in Runge, 2007; lithostratigraphy after Baudet et al., 2018b). River samples are indicated, together with the dominant heavy minerals in each tributary sand (Ep = epidote; Ky = kyanite; ZTR = zircon + tourmaline + rutile).

(Fig. 3), channel depth reaches ≥220 m making this fluvial section the deepest on Earth (Oberg et al., 2009). About 40 km upstream of Matadi are located the Inga Falls, the largest rapids in the world, where water rushes at 14 m/s, waves are up to 12 m in height, and channel steepness reaches extreme values (Fig. 4). Two large hydropower plants are operative at Inga (dam closure in 1972 and 1982), where the Great Inga project, if completed, will represent the largest hydropower plant on Earth with an energy-generation potential twice as that of the Three Gorges Dam on the Yangtze River in China (Showers, 2009).

In the 134 km-long navigable stretch from Matadi to the mouth, the river is at first narrow, characterized by huge whirlpools, and deeply incised for up to 250 m into exposed quartzite. It next widens to 19 km with very large active sand bars, to finally become an estuary with average tidal range of 1.4 m downstream of Boma (Bultot, 1971).

Some 30 km upstream of the mouth, the river channel deepens into a submarine valley directly connected with a huge canyon deeply entrenched into the continental shelf and continuing for ~760 km downslope of the coast to water depths of ~5000 m b.s.l. As a consequence, the Congo River has no subaerial delta and virtually its entire bedload reaching the sea is ultimately transferred directly by turbidity currents to the huge Congo Fan, as documented by repeated cable breaks in the canyon coinciding with periods of peak water and sediment discharge (Heezen et al., 1964; Babonneau et al., 2010; Anka et al., 2009). Frequent and powerful mud-rich turbidity flows, possibly triggered by slope instability, are prolonged over several days to a full week. Active turbiditic sedimentation during the current interglacial highstand is a peculiar feature that distinguishes the Congo from the other major rivers on Earth (Babonneau et al., 2002). Sediment

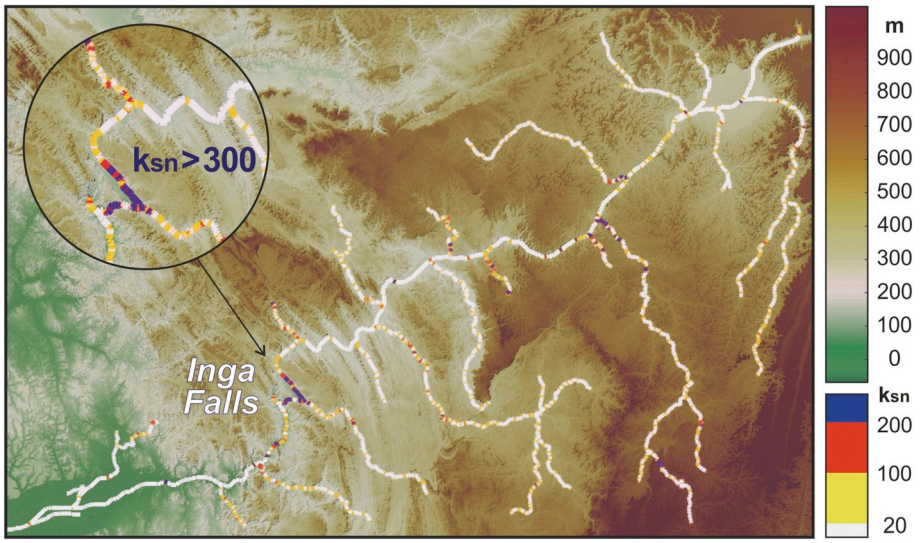

Fig. 4. Topographic relief and morphometry of the Congo River in Bas-Congo (elevation in m a.s.l.). Channel-profile analysis emphasizes the extreme steepness values reached in the Inga Falls (*ksn* up to 800 at the bend), a most prominent knickpoint associated with recent uplift of the Atlantic Rise and sharp lithological contrast between the Lufu microgranite-gneiss massif (Kianga facies of Tack, 1973) and its Inga metavolcanic wallrocks (Duizi-Inga series of Tack, 1973).

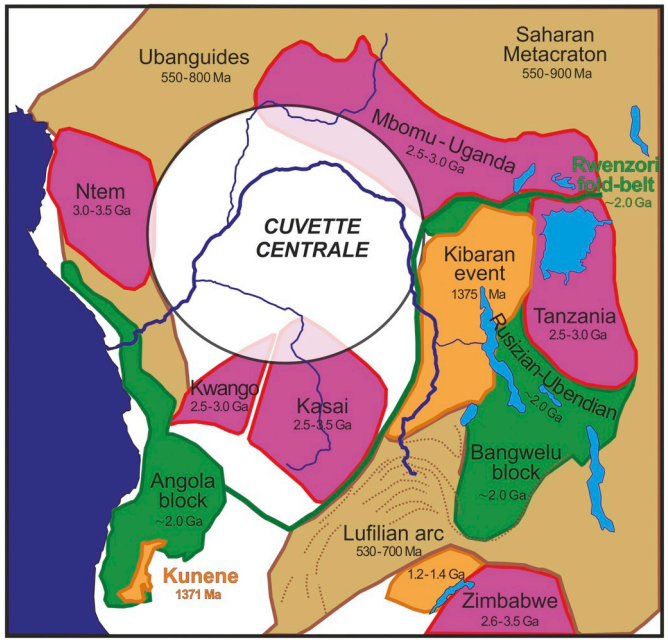

Fig. 5. Schematic map of central Africa (modified after Fig. 2.5 in de Wit and Linol, 2015) showing diverse Archean cratonic blocks (purple), Paleoproterozoic (Eburnean) fold-belts (green), domains affected by Mesoproterozic intrusions (orange), and Pan African fold-belts (light brown). Ages of Precambrian basement units surrounding the central Congo basin are indicated. (For interpretation of the references to colour in this figure legend, the reader is referred to the web version of this article.)

transport is of the same order of magnitude as the discharge of the Congo River, and involves an estimated ~2% of the total terrestrial organic carbon buried annually in the world's oceans (Azpiroz-Zabala et al., 2017).

The Congo canyon, lying 480 m b.s.l. at the river mouth and ~1000 m b.s.l. at the shelf edge, cuts across salt diapirs and continues into a meandering channel over a cumulative length of 1135 km from the estuary to the fan lobes (Savoye et al., 2000). Congo turbidites are thus traced for > 1000 km, whereas during hypopycnal flows the sediment-laden surface plume can be followed for 20 km and the freshwater plume to as far as 800 km offshore (Eisma and Kalf, 1984; Braga et al., 2004; Denamiel et al., 2013).

The deep trench impressively carved by the Congo River across the entire width of the western African continental margin, from the recently uplifted Atlantic Rise in Bas-Congo to the huge deep-sea canyon offshore, is a unique geomorphic feature, the origin, causal mechanisms, and evolution of which are still poorly understood (Ferry et al., 2004; Anka et al., 2010). Diverse and complexly interplaying factors controlling the balance between erosion and sedimentation have been called upon, including tectonic activity and climatic, eustatic, and oceanographic changes (Séranne and Anka, 2005). Lavier et al. (2001) pointed out that global cooling at the Eocene/Oligocene transition and related onset of Antarctic intermediate-depth oceanic currents, coupled with Miocene epeirogenic uplift of Africa, may have triggered submarine erosion and mass wasting. McGinnis et al. (1993) documented truncation of seismic reflectors associated with this event, indicating prominent deep-sea erosion, slope retreat, and canyon cutting across the outer shelf and slope, and emphasized the role of erosional unloading to promote flexural rebound and uplift of the continental margin. Lucazeau et al. (2003) related instability of drainage and migration of depocenters from the Ogooué and Kwanza Rivers to the Congo Fan in the Oligocene to regional flexural rebound and Miocene uplift of the continental margin by ≤450 m. Cramez and Jackson (2000) suggested that fault control on the Congo Canyon may have been exerted by Neogene inversion and reactivation of a sub-salt half-graben. Séranne and Anka (2005) related increased erosion and development of the huge Congo Fan to northward plate motion whereby the Congo catchment, previously characterized by arid tropical conditions, reached the wet equatorial belt in the Neogene. A positive feedback of fluvial incision and canyon cutting followed by erosional unloading, possibly initiated with "dynamic" uplift of Africa and climate change in the Oligocene, may have culminated with capture of the vast endorheic Congo catchment by a headward-eroding coastal stream. Submarine erosion, related either to gravity flows triggered by sediment overload and failure at the head and flanks of the canyon or to hyperpycnal currents generated by fluvial floods, continued throughout the Neogene. Enhanced further during Pleistocene glacio-eustatic lowstands, it has remained active until today (Shepard and Emery, 1973; Savoye et al., 2009; Dennielou et al., 2017).

2.2. Hydrology and sediment load

The Congo River is second on Earth only to the Amazon in drainage area and water discharge (minimum 23,000 m^3/s, mean 41,000 m^3/s, maximum 75,500 m^3/s; Laraque et al., 2009, 2013). Two flow regimes exist in the huge catchment. The Ubangui and other tributaries draining sub-humid regions north of the Equator reach maximum discharge between September and November, and minimum in February to April. In contrast, southern tributaries reach maximum discharge at different times between March and May, and minimum in September–November. As a consequence, the trunk river records peak discharge around December, after receiving the rainy-season runoff from the Ubangui, and a smaller peak fed from southern branches around May. Discharge variability through the year is reduced by regularly high rainfall in the central Congo basin. Because of scarce industrial activities and huge discharge, river waters are relatively unpolluted.

The Congo River is estimated to carry ~30 10^6 t/a suspended load (~8 10^6 t very fine sand, ≥ 20 10^6 t silt and clay, ≤ 3 10^6 t organic matter), a figure which is only a half of total dissolved material (58 10^6 t, ~27% of which derived from organic matter; Laraque et al., 1995, 2009). Sediment yield is thus ≤10 t km^{-2} a^{-1}. Suspended load has low concentration (average 25 mg/l; Laraque et al., 2013) and includes clay (~50% kaolinite, ~25% illite, ≤10% each smectite, chlorite, and mixed layers), mostly fine to medium silt, organic matter, amorphous silica, phytoliths, and Fe-oxy-hydroxides (Eisma et al., 1978). The dissolved load largely consists of silica and bicarbonate, largely supplied by the Ubangui River which drains Precambrian limestone and carries ~80% kaolinite, ~20% illite, and little smectite (Delaune et al., 1995; Laraque and Olivry, 1996).

2.3. Geology and geomorphology

The oval-shaped *cuvette centrale*, ~1000 km in diameter and once possibly occupied by a huge lake (Peters and O'Brien, 2001), lies at elevations between 300 and 500 m a.s.l. surrounded by hilly reliefs formed by deeply-weathered Precambrian to Mesozoic rocks. One of the largest intracratonic basins on Earth, the *cuvette centrale* is underlain by crystalline basement of the Congo craton, consisting of several Archean blocks welded during the Paleoproterozoic Eburnean orogeny (Fig. 5; Cahen et al., 1984; De Waele et al., 2008; de Wit and Linol, 2015). The overlying strata comprise Neoproterozoic schist, quartzite, evaporite, and carbonate locally folded during the Pan-African orogeny and unconformably overlain by ~1 km-thick, tabular, feldspar-rich Paleozoic redbeds (Delpomdor and Préat, 2015). Permo-Carboniferous deposits including tillite, sandstone, and coal-bearing lacustrine sediment (~1.5 km-thick Karoo Supergroup; Linol et al., 2015b) are overlain by ~1 km of quartz-rich sandstone, silt, bituminous shale, and lacustrine limestone deposited under variable climatic conditions during the Mesozoic and Cenozoic (Linol et al., 2015c; Roberts et al., 2015; Agyemang et al., 2016). A major hiatus encompasses part of the Triassic

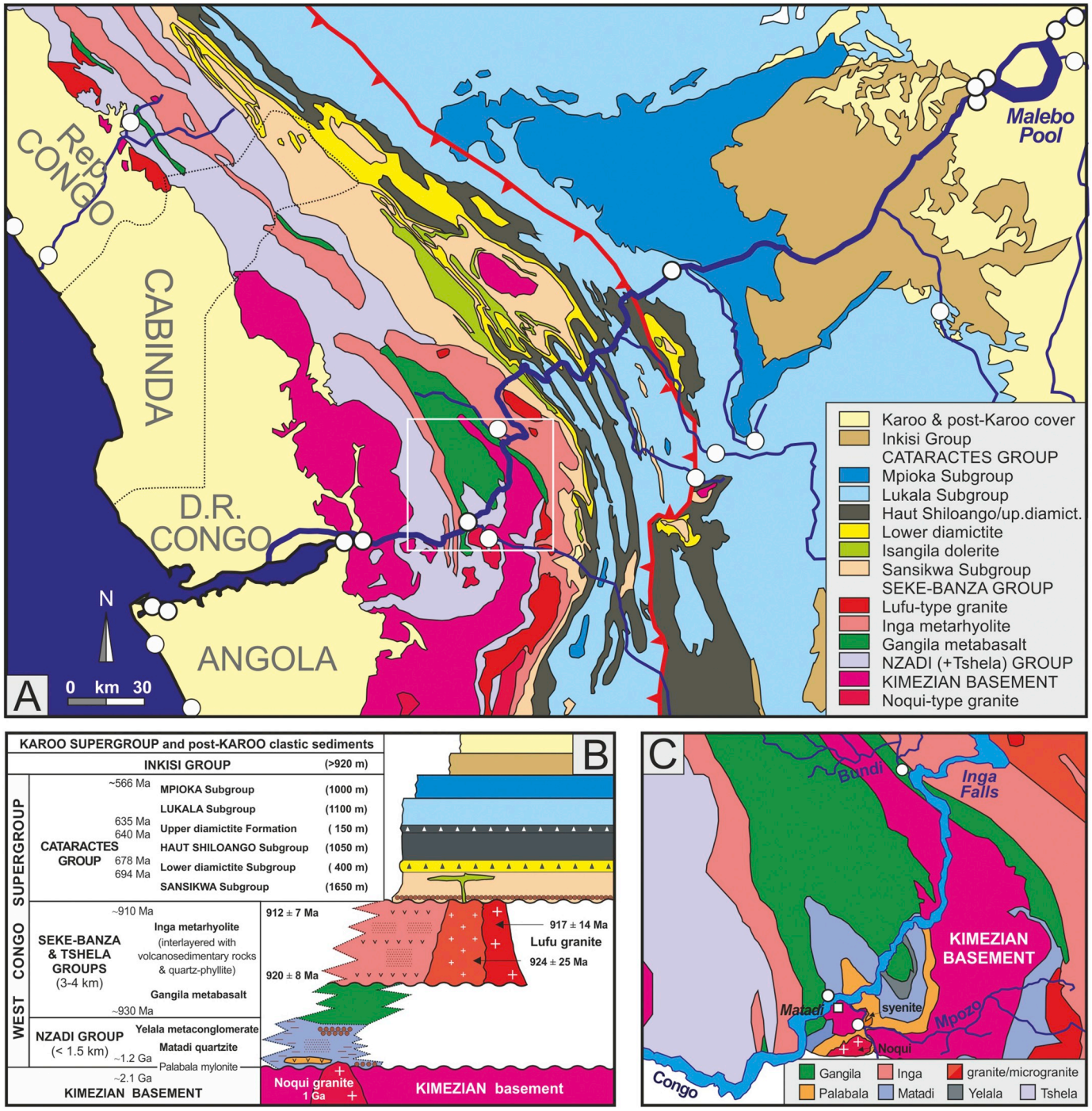

Fig. 6. The West Congo belt in Bas-Congo (after Tack et al., 2001; updated lithostratigraphy after Baudet et al., 2018b). (A) Regional geological map (the white rectangle outlines the area enlarged in C; white circles indicate sampling sites). (B) Lithostratigraphic framework. (C) Geological map of the Matadi region (after Tack, 1975).

and the Early Jurassic (Kadima et al., 2011).

In the north, the Congo craton exposed along the Asande Rise is drained by the Ubangui River and its Uele, Mbomu, and Kotto branches (Fig. 2). It includes a Mesoarchean amphibole-gneiss complex (2.9–3.2 Ga) and granitoid intrusions (2.84–3.2Ga) overlain by Proterozoic marble and quartzite (Cahen et al., 1984; CGMW-BRGM, 2016). In the east, recently uplifted highlands along the western branch of the East African rift reach maximum elevations of 3308 m, 4507 m, and 5110 m a.s.l. in the Mitumba Mountains cored by Neoproterozoic alkaline granite, in volcanoes of the Neogene potassic Virunga province, and in the Paleoproterozoic Rwenzori crystalline massif, respectively. In the south, basement rocks of the Kasai shield reach an elevation of 1800 m a.s.l. in the Angola and Shaba highlands. They consist of Mesoarchean to Paleoproterozoic granite, gneiss, migmatite, and gabbro dated between 2.0 and 3.4 Ga, overlain by ≥6 km-thick metasedimentary rocks and metalavas dated between 1155 and > 1400 Ma (Cahen et al., 1984).

In Bas-Congo, from the Malebo Pool to the Atlantic Ocean, the Congo River cuts across the West Congo belt, a recently rejuvenated, eastward-verging Neoproterozoic (Pan-African) orogen extending parallel to the coast between northern Angola and Gabon for ~1300 km in length and 150–375 km in width (Fig. 6A; Frimmel et al., 2006;

Pedrosa-Soares et al., 2008; Affaton et al., 2016). The crystalline basement, represented by gneiss, migmatite, and amphibolite deformed at ~2.1 Ga during the Eburnean (Kimezian) orogeny, is thrust eastward onto Neoproterozoic tectono-stratigraphic units displaying eastward-decreasing metamorphic grade from amphibolite facies to unmetamorphosed strata in the foreland. The contact between the Kimezian basement and the overlying metasedimentary rocks of the Nzadi (formerly Zadinian) Group, including the upper Mesoproterozoic Matadi quartzite and Yelala metaconglomerate (Baudet et al., 2018a), is marked by mylonitic rocks from diverse protoliths originally described as the "Palabala Formation" (Tack, 1975; Franssen and André, 1988). Igneous rocks exposed near Matadi include the Mpozo syenomonzonite of Eburnean age (1948 ± 10 Ma) and the Noqui peralkaline granite, intruded into Matadi quartzite at ~1 Ga (Fig. 6C; De Grave et al., 2018). The 3–4 km-thick, lower Tonian Seke-Banza Group comprises the Gangila metabasalt and the Inga metarhyolite, which includes felsic volcanic and volcaniclastic rocks locally intercalated with quartzite and quartz-phyllite (Fig. 6B; Baudet et al., 2018b). The Seke-Banza (formerly Mayumbian) Group, dated at 920 ± 8 Ma at the base and at 912 ± 7 Ma at the top, was intruded by monzogranite to syenogranite and alkali-feldspar granite also dated at ~920 Ma. The Nzadi and Seke-Banza Groups may represent a continental rift sequence with initial peralkaline magmatism followed by extensive bimodal magmatism (Tack et al., 2001).

The Seke–Banza Group is overlain by the Neoproterozoic Cataractes Group, which includes ~4 km-thick siliciclastic, diamictite, and carbonate strata deposited before the climax of the Pan-African orogeny (Cryogenian Sansikwa and Haut-Shiloango Subgroups, and Ediacaran Lukala Subgroup), and the ~1 km-thick Mpioka Subgroup deposited at late Ediacaran times in the foreland of the Pan-African orogen (Cailteux et al., 2015). The Sansikwa Subgroup consists of ~1650 m-thick continental siliciclastic sediments overlain by the ~400 m-thick Lower Diamictite Formation, which might be correlated globally with the Sturtian glaciation (717–660 Ma; Hoffman and Li, 2009; Rooney et al., 2015). The occurrence of glacigenic features is however disputed, and the occurrence of interbedded tholeiitic basalt has suggested episodic extensional activity associated with the breakup of Columbia (Archibald et al., 2018). Deposition is constrained to have taken place around 694 ± 4 Ma by U—Pb baddeleyite dating of a doleritic feeder dyke (Straathof, 2011) and before 678 ± 4 Ma by detrital-zircon chronostratigraphy (Archibald et al., 2018). The overlying Haut-Shiloango Subgroup, consisting of ~1 km-thick siliciclastic sediments and subordinate carbonate rocks at the top, is capped by the 150–200 m-thick Upper Diamictite Formation, which may be correlated globally with the Marinoan glaciation (639–635 Ma; Macdonald et al., 2010; Prave et al., 2016) although the occurrence of glacigenic features is disputed. The ~1 km-thick Lukala (formerly Schisto-Calcaire) Subgroup includes shelfal marly, oolitic, and stromatolitic limestone and dolostone (Delpomdor et al., 2015). The ~1 km-thick Mpioka Subgroup siliciclastic rocks are considered as the molasse of the Pan-African orogen, themselves involved in orogeny at ~566 Ma (Frimmel et al., 2006). The deformed rocks of the West Congolian Supergroup are unconformably overlain by the > 900 m-thick redbeds of the Paleozoic Inkisi Group.

After prolonged phases of erosion and peneplanation (Veatch, 1935), the rapid uplift responsible for the markedly juvenile character of the lower course of the Congo River began in the late Paleogene, when the *cuvette centrale* still lay close to sea level, and accelerated toward the close of the Miocene (Guillocheau et al., 2015). Offshore, Eocene deep-water carbonate sedimentation was interrupted by submarine erosion of ≤1 km of sediment from the shelf break and upper slope, followed by a drastic increase in sediment supply leading to progradation and shallowing (Lavier et al., 2001). Turbidite sedimentation started at early Oligocene times, followed by incision of the Congo canyon and basinward progradation of the fan onto the abyssal plain while deposition on the slope remained dominated by hemipelagic mud (Anka et al., 2009).

3. Sampling and analytical methods

Between June 2015 and October 2016, we collected 14 sand samples along the Congo River and its lower course tributaries in Bas-Congo, from just upstream of the Malebo (Stanley) Pool to the estuary, and 2 estuary channel and beach sands at Soyo in Angola. Although the central part of the huge basin could not be accessed, 16 additional samples were collected in previous and subsequent years on the Congo River at Brazzaville, in upstream parts of the catchment on its Ubangui tributary at Bangui, in the Ruizi and Malagarazi catchments in Burundi and Tanzania, and along the Atlantic coast from northern Angola to the Republic of Congo and Gabon. Moreover, we analysed 5 offshore samples from the adjacent shelf and Congo Fan, collected within 1 m below the seafloor at water depths between −30 and −3100 m b.s.l. during Meteor expeditions M6/6, M20/2, and M76/3a and retrieved from the MARUM repository in Bremen (Wefer et al., 1988; Schulz et al., 1992; Spiess and Shipboard Party, 2012). This set of 37 samples allowed us to investigate the compositional signatures of sediment produced in subequatorial Africa and the relative importance of weathering and recycling in the generation of pure quartzose sand. Full information on sampling sites is provided in Appendix Table A1 and Google Earth™ file *Congo.kmz*.

3.1. Petrography and heavy minerals

A quartered fraction of each sample was impregnated with Araldite, cut into a standard thin section stained with alizarine red to distinguish dolomite and calcite, and analysed by counting between 400 and 500 points by the Gazzi-Dickinson method (Ingersoll et al., 1984). Sand is classified according to the three main groups of framework components (Q = quartz; F = feldspars; L = lithic fragments), considered where exceeding 10%QFL and listed in order of abundance (classification scheme after Garzanti, 2019). Feldspatho-quartzose sand is thus defined as Q > F > 10%QFL > L, formally distinguishing between feldspar-rich (Q/F < 2; plagioclase-rich if plagioclase/K-feldspar > 2, K-feldspar-rich if K-feldspar/plagioclase > 2) and quartz-rich (Q/F > 4) compositions. Quartzose sand is defined as Q/QFL > 90%, and pure quartzose sand as Q/QFL > 95%. These subtle distinctions proved to be essential to discriminate among siliciclastic sediments deposited along passive continental margins in different tectonic and climatic settings (Garzanti et al., 2018a). Microcline with cross-hatch twinning is called for brevity "microcline" through the text. Median grain size was determined in thin section by ranking and visual comparison with standards of ϕ/4 classes prepared by sieving in our laboratory.

From a split aliquot of the widest convenient size-window obtained by wet sieving (mainly 15–500 μm), heavy minerals were separated by centrifuging in Na-polytungstate (2.90 g/cm^3) and recovered by partial freezing with liquid nitrogen. In grain mounts, ≥ 200 transparent heavy minerals for each sample were either point-counted at appropriate regular spacing to obtain correct volume percentages or grain-counted by the area method (Galehouse, 1971). On silt-sized offshore samples, mineralogical analyses were carried out by coupling observations under the microscope and Raman counting (Andò et al., 2011) on both low-density (< 2.90 g/cm^3) and high-density (> 2.90 g/cm^3) fractions of the > 15 μm class. Transparent heavy-mineral assemblages, called for brevity "tHM suites" throughout the text, are defined as the spectrum of detrital extrabasinal minerals with density > 2.90 g/cm^3 identifiable under a transmitted-light microscope. According to the transparent-heavy-mineral concentration in the sample (tHMC), tHM suites are defined as very poor (tHMC < 0.5), poor (0.5 ≤ tHMC < 1), moderately poor (1 ≤ tHMC < 2), moderately rich (2 ≤ tHMC < 5), rich (5 ≤ tHMC < 10), or very rich (tHMC >

10) (Garzanti and Andò, 2007, 2019). The sum of zircon, tourmaline, and rutile over total transparent heavy minerals (ZTR index of Hubert, 1962) expresses the chemical durability of the tHM suite (Garzanti, 2017). In all analysed samples, corrosion features were assessed systematically by three different operators on ~4200 transparent heavy-mineral grains, following the classification of surface textures in Andò et al. (2012). Significant minerals are listed in order of abundance (high to low) throughout the text. Key compositional parameters are summarized in Table 1. The complete petrographic, heavy-mineral, and surface-texture datasets are provided in Appendix Tables A2, A3, and A4.

3.2. Geochemistry

Chemical analyses of a quartered aliquot of the 63–2000 μm class obtained by wet sieving from 13 sand samples from the Congo River and its tributaries, together with 7 coastal beach and river sands from northernmost Angola, the Republic of Congo, and Gabon were carried out at Bureau Veritas Mineral Laboratories (Vancouver, Canada). Following a lithium metaborate/tetraborate fusion and nitric acid digestion, major oxides and several minor elements were determined by ICP-ES and trace elements by ICP-MS (see Appendix A for specific information on the adopted analytical protocol).

Several chemical indices may be used to estimate weathering, including the Chemical Index of Alteration [$CIA = 100 \cdot A1_2O_3/(A1_2O_3 + CaO + Na_2O + K_2O)$] (Nesbitt and Young, 1982) and the Weathering Index [$WIP = 100 \cdot (CaO/0.7 + 2Na_2O/0.35 + 2K_2O/0.25 + MgO/0.9)$] (Parker, 1970), calculated using molecular proportions of mobile alkali and alkaline earth metals corrected for CaO in apatite. Instead of correcting the CIA for CaO in carbonates based on mineralogical data, which may result in significant error (Garzanti and Resentini, 2016), wherever carbonate grains are present we prefer to use the CIX index, a simple modification of the CIA that does not consider CaO [$CIX = 100 \cdot A1_2O_3/(A1_2O_3 + Na_2O + K_2O)$] (Garzanti et al., 2014a, 2014b). Weathering intensities can be calculated also for each single mobile element separately, by comparing its concentration to that of non-mobile Al in our samples and in the Upper Continental Crust (UCC standard after Taylor and McLennan, 1995; Rudnick and Gao, 2003): $\alpha^{Al}E = (Al/E)_{sample}/(Al/E)_{UCC}$ (Garzanti et al., 2013a, modified after α values of Gaillardet et al., 1999). Rare earth elements (REE) were normalized to CI carbonaceous chondrites (McDonough and Sun, 1995); the relative contribution to REE distributions by different minerals was interpreted based on their typical REE patterns (as in Fig. 5 of Garzanti et al., 2011). Key elements and weathering indices are shown in Table 2. The complete geochemical dataset is provided in Appendix Table A5.

3.3. Detrital geochronology

Detrital zircon was separated from quartz and feldspar using bromoform, and from (para)magnetic heavy minerals using a hand magnet and a Frantz magnetic separator. U−Pb ages were determined at the London Geochronology Centre using an Agilent 7700× laser ablation-inductively coupled plasma-mass spectrometry (LA-ICP-MS) system, employing a NWR193 Excimer Laser operated at 11 Hz with a 25 μm spot size and 2.5–3.0 J/cm^2 fluence. Because our main goal was to compare different age distributions with each other like fingerprints, no cathodo-luminescence imaging was done and the laser spot was always placed "blindly" in the interior of zircon grains to treat all samples in exactly the same way ("blind dating strategy" of Garzanti et al., 2018b). The mass spectrometer data were converted to isotopic ratios using GLITTER 4.4.2 software (Griffin et al., 2008), employing Plešovice zircon (Sláma et al., 2008) as a primary age standard and GJ-1 (Jackson et al., 2004) as a secondary age standard. NIST SRM612 was used as a compositional standard for the U and Th concentrations. GLITTER files were post-processed in R using IsoplotR 2.5 (Vermeesch, 2018a). Age distributions were calculated by: (i) removing grains with a precision of worse than 10%; (ii) removing grains with > +5/−15% age discordance; and, (iii) applying a Stacey-Kramers correction to the remaining measurements (Chew et al., 2014). This procedure yielded over 1500 concordant ages from 14 samples. In analogy with previous articles in the region (Garzanti et al., 2017a, 2018a), the five age clusters recurring in the analysed samples are named Karoo (240–295 Ma; Permo-Triassic), Pan-African (0.5–0.65 Ga, late Neoproterozoic), Seke-Banza (0.9–1.1 Ga, Stenian-Tonian), Eburnean (mid-Paleoproterozoic; 1.9–2.1 Ga), and Neoarchean (2.5–2.7 Ga). The complete geochronological dataset is provided in Appendix B.

3.4. Channel-profile analysis

The geomorphic features characterizing the course of the Congo River in Bas-Congo were quantified using TopoToolbox, a set of MATLAB functions for the analysis of relief and flow pathways in digital elevation models (DEM; Schwanghart and Scherler, 2014). Channel-profile analysis was carried out on a 30 m-resolution DEM provided by Shuttle Radar Topography Mission Global (SRTM GL1; https://opentopography.org) to identify major knick-points, defined as sites where the channel gradient changes abruptly owing to a sharp local change in bedrock strength and/or uplift rate. Normalized channel-steepness indices (k_{sn}) were calculated from the power-law relationship $S = k_s A^{-\theta}$ between local channel slope S and contributing drainage area A (a proxy for discharge; Hack, 1957; Flint, 1974). A fixed reference concavity ($\theta_{ref} = 0.45$) was used to facilitate comparisons among channel slopes with widely varying drainage areas and concavities (Snyder et al., 2000; Whipple, 2004; Wobus et al., 2006; Norton and Schlunegger, 2011).

4. Results

In this section, petrographic, heavy-mineral, geochemical and geochronological data are presented subdivided by geographic area, from the upper course upstream of the *cuvette centrale* (Fig. 5) to the lower course in Bas-Congo (now Kongo Central province; Fig. 1), the Atlantic coast, the shelf, and the deep sea. Petrographic parameters used below include the Qp/Q (polycrystalline/total quartz) and P/F (plagioclase/total feldspar) ratios.

4.1. Upper course tributaries

The Congo catchment is huge and largely difficult to access. Our sample coverage of the numerous tributaries is consequently limited to a few rivers in the upper catchment, i.e., the Ubangui and the Rusizi and Malagarasi upstream of Lake Tanganyika.

Upstream of the *cuvette centrale*, the Ubangui River largely drains Archean to lower Paleoproterozoic granitoid gneiss and granulite of the Congo craton, and carries quartz-rich feldspatho-quartzose sand with K-feldspar (including common microcline) > plagioclase, a few quartzose siltstone and granitoid rock fragments, mica (muscovite ≈ biotite), and a poor tHM suite including kyanite with subordinate staurolite and blue-green to green-brown hornblende, minor epidote, mainly prismatic sillimanite, rutile, tourmaline, garnet, and clinopyroxene.

The Rusizi River drains medium-grade to high-grade mid-Paleoproterozoic (2.1–2.0 Ga) gneiss of the Rusizian-Ubendian belt exhumed around 1.85 Ga (Boven et al., 1999) and basalt, trachyte and phonolite of the South Kivu volcanic field emplaced during Neogene rifting (Furman and Graham, 1999). Sand entering Lake Tanganyika is quartz-rich feldspatho-quartzose with K-feldspar (including common microcline) > plagioclase and minor basaltic and high-rank metasedimentary and metaigneous rock fragments. Mica is common (muscovite > biotite). The moderately poor tHM suite includes dominant blue-green to green amphibole with subordinate tourmaline and minor prismatic or fibrolitic sillimanite, garnet, epidote, and staurolite (Table 1).

Table 1
Petrography and heavy minerals in Congo sands.

River @ Site	Sample	Q	KF	P	Lvm	Lc	Lh	Lpm	Lm	mica	HM		$tHM_{w\%}$	ZTR	&Tiox	Ttn	Ap	Mon	Ep	Grt	St	And	Ky	Sil	Amp	Cpx	Hy	&tHM	
Upper course tributaries																													
Malagarasi @ Ilagala	S3837	81	1	2	13	0	0	3	0	0	0	100.0	0.3	32	4	0	0	1	26	1	2	13	0	2	20	0	0	0	100.0
Rusizi @ Gatumba	S3856	71	12	5	2	0.2	0	0	2	5	3	100.0	1.8	18	5	0	0	0	4	5	3	0	0	8	56	0	0	0.5	100.0
Ubangui @ Bangui	S5147	75	11	7	0	0	0	0	0	1	6	100.0	0.7	12	0	0	0	0	8	3	13	0	47	6	10	2	0	0	100.0
Bas-Congo tributaries																													
Nsele @ E Kinshasa	S5208	97	1	0.3	1	0	0	0	0	0.3	1	100.0	0.3	87	2	0	0	0	1	0	6	0	3	0	0.5	0	0	0.5	100.0
Inkisi @ Kisantu	S5209	97	0.3	0	1	0	0.3	0.3	0.3	0	1	100.0	0.9	12	0	0	0	0	3	8	5	0	72	0	0	0	0	0	100.0
Lunkunga @ Komoina	S5210	90	1	1	0.3	0	1	5	1	0	0	100.0	0.1	85	13	0	0.4	2	0	0	0	0	0	0	0	0	0	0	100.0
Kwilu @ Kwilu	S5211	84	2	3	2	0	3	4	1	0	1	100.0	0.3	82	13	0	0.4	1	0.4	0	0.4	0	2	0	0.4	0	0	0	100.0
Mbangala @ Vunda	S5217	34	1	2	0	0	0	56	6	1	0	100.0	1.6	94	3	0	0	1	3	0	0	0	0	0	0	0	0	0	100.0
Bundi @ Inga	S5212	66	7	8	1	0	0	5	5	0.3	8	100.0	8.4	2	0	0	0	0	94	0	0	0	0	0	5	0	0	0	100.0
Mpozo @ Matadi	S5213	73	9	6	0.2	0	0	2	3	3	4	100.0	2.3	33	0	0.5	0	0	41	1	0	0	0.5	0.5	23	0	0	0	100.0
Congo River in Bas-Congo																													
Congo @ Gafura	S5206	99	0	0	0	0	0.3	0	0	0	0	100.0	0.2	79	0.5	0	0	0	1	0	9	1	2	3	2	1	0	1	100.0
Congo @ Linda	S5207	99	0	0	0	0	0	0	0	0	1	100.0	0.1	68	4	0	0	0	8	0	9	0	2	2	3	2	0	1	100.0
Congo @ Brazzaville	S3533	97	2	0	0.3	0	0	0	0	0	0.3	100.0	0.0	49	2	0	0	1	14	4	17	1	9	0	4	0	0	0	100.0
Congo @ Brazzaville	S5148	93	4	1	0	0	0	0	0	0	2	100.0	0.2	61	0	0	0	0.5	7	4	14	0	6	2	4	1	0	0	100.0
Congo @ Kinshasa	S5114	98	1	0	0	0	0	0.3	0	0	1	100.0	0.2	78	0	0	0	0.4	6	2	10	0	2	0	2	0.4	0	0	100.0
Congo @ Luozi	S5216	93	2	1	0	0	0	0.2	0	1	1	100.0	0.5	66	2	0	1	0	11	2	1	0	5	3	8	0	0	0.5	100.0
Congo @ Matadi	S5214	97	1	0.3	0.3	0	0	0.3	1	0	1	100.0	0.1	69	0	0	0	0	9	3	7	0	5	1	5	0	0	0	100.0
Congo @ Boma	S5215	88	7	2	1	0	0	1	1	0.3	1	100.0	0.5	67	2	0	0	0.5	12	3	5	0	1	1	5	2	0	0.5	100.0
Congo @ Isle de Mateba	S5115	97	1	1	0	0	0	0	0	0	1	100.0	0.3	44	0	0.5	0	0	20	2	15	0	10	3	5	0	0.5	0	100.0
Estuary channel @ Soyo	S4899	98	1	1	0	0	0	0	0	0	0.3	100.0	0.3	36	0	0.5	0.5	0	8	3	9	0	33	0.5	10	0	0	0	100.0
Estuary beach @ Soyo	S4898	98	1	1	0	0	0	0	0	0.3	0	100.0	0.1	47	0	1	1	0	19	2	5	1	7	3	13	0	0	0	100.0
Atlantic coast																													
Akwengo Bay beach	S5617	97	1	0.3	0.3	0	0	1	0	0	0	100.0	0.09	67	0	0	1	0	2	10	12	0	4	1	2	1	0	0	100.0
Libreville beach	S5530	92	7	1	0	0	0	0	0	0	0	100.0	0.09	79	0	0	4	0	1	6	2	0	1	0	6	0.5	1	0	100.0
SW Port Gentil beach	S5618	98	1	0.3	0	0	0	0	0	0	0.3	100.0	0.24	57	0	0	0	0	1	1	24	1	14	1	1	0	0	0	100.0
Pointe Noire beach	S0162	99	1	0	0	0.1	0	0.1	0	0	0	100.0	0.3	67	0.3	0	0	0	1	0	13	0.3	18	1	0	0	0	0	100.0
Loussoni River	S4053	99	0	0	0	0	0	1	0	0	0.3	100.0	0.01	77	0	0	4	0	3	9	6	0	1	0	0	0	0	0	100.0
Loémé River	S0161	99	0.3	0	0	0	0	0	0	0	1	100.0	0.5	71	0.4	0	0	0	8	0	10	1	10	0	0	0	0	0	100.0
Quimtomba beach	S4901	97	1	1	0	0.3	0	0	0	0	0.3	100.0	1.3	13	0	0	1	0	31	13	9	0	17	0	16	0	0	0	100.0
Quifuma beach	S4902	95	3	1	0	0	0	0	0	0	1	100.0	0.8	5	0	0.5	0	0	39	13	5	0	15	0	22	0	0	0	100.0
Quivanda beach	S4903	88	6	3	0	0	0	0	0.3	0	3	100.0	3.1	4	0	0	0	0	30	24	0.4	1	9	0	32	0	0	0	100.0
Luculu river mouth	S4904	86	4	5	0	0	0	0	0	0.3	5	100.0	5.1	7	0	1	0	0	30	33	2	0	15	0	13	0	0	0	100.0
Mbua-Moyo beach	S4905	90	5	4	0	0	0	0.3	0	0	2	100.0	3.6	3	0	1	1	0	46	19	1	0	6	0	23	0	0	0	100.0
Shelf & deep sea																													
Congo shelf	GeoB1004–3	82	5	3	0.4	0	0	0	0	0	10	100.0	2.4	19	0	0	1	0	29	23	0	0	8	2	19	0	0	0	100.0
S of Congo Canyon	GeoB13109A	70	10	20	0	0	0	0	0	0	0.1	100.0	0.0	15	0	1	4	0	21	1	1	0	4	4	24	12	4	7	100.0
S of Congo Canyon	GeoB13109B	64	7	14	0	1	0	0	0	1	14	100.0	0.3	9	0	0	9	0	35	0	0	0	0	0	4	17	26	0	100.0
N of Congo Canyon	GeoB13115A	62	0	30	0	0	0	0	0	2	6	100.0	0.6	4	0	0	0	0	5	1	0	0	0	0	12	31	47	0	100.0
N of Congo Canyon	GeoB13115B	72	4	21	0	0	0	0	0	0	2	100.0	0.1	14	0	0	1	0	7	2	0	1	0	0	12	40	19	3	100.0

Q = quartz; KF = K-feldspar; P = plagioclase; L = aphanitic lithic grains (Lvm = volcanic and metavolcanic; Lc = carbonate; Lh = chert; Lpm = pelite and low-rank metapelite; Lm = high-rank metamorphic; $tHM_{w\%}$ = transparent heavy minerals (weight %); ZTR = zircon + tourmaline + rutile; &Tiox = other Ti-oxides (mainly anatase); Ttn = titanite; Ap = apatite; Mon = monazite; Ep = epidote; Grt = garnet; St = staurolite; Ky = kyanite; Sil = sillimanite; Amp = amphibole; Cpx = clinopyroxene; Hy = hypersthene; &tHM = other transparent heavy minerals (chloritoid, Cr-spinel, olivine, enstatite, barite, corundum).

Table 2
Geochemistry of Congo sands. The Si/Zr ratio is ~1600 in the UCC standard (Taylor and McLennan, 1995; Rudnick and Gao, 2003) and ~12,600 in commercial silica used in our lab, which is thus less pure than Pointe Noire and Libreville beach sand! Chemical weathering indices as defined in Section 3.2. The Z/(Z + T) ratio (Z = zircon; T = tourmaline) is proposed here as an index of hydraulic sorting in quartz-rich sand and sandstone; n.d. = not determined.

River @ Site	Sample	SiO_2	Zr	Si/Zr	CIA	CIX	WIP	$\alpha^{Al}Mg$	$\alpha^{Al}Ca$	$\alpha^{Al}Na$	$\alpha^{Al}K$	$\alpha^{Al}Rb$	$\alpha^{Al}Sr$	$\alpha^{Al}Ba$	Z/(Z + T)
		wt%	ppm												
Upper course tributaries															
Malagarasi @ Ilagala	S3837	88.1	92	4456	61	70	13	0.9	1.8	2.5	0.8	0.8	2.9	0.9	46%
Rusizi @ Gatumba	S3856	84.6	106	3750	60	64	28	1.4	3.5	1.5	0.7	0.6	2.7	0.8	9%
Bas-Congo tributaries															
Inkisi @ Kisantu	S5209	97.8	103	4432	87	91	1	2.9	6.1	22.5	2.8	3.0	3.8	1.1	77%
Lunkunga @ Komoina	S5210	96.6	147	3063	71	79	3	0.7	2.6	8.0	1.0	0.9	1.6	0.9	52%
Mbangala @ Vunda	S5217	84.4	123	3212	76	75	14	2.4	14.9	30.9	0.7	0.5	8.8	0.9	32%
Bundi @ Inga	S5212	87.8	319	1287	49	67	20	4.2	0.8	1.7	0.8	1.0	1.3	0.8	100%
Mpozo @ Matadi	S5213	89.7	399	1050	54	60	21	3.0	2.4	1.2	0.6	0.7	2.0	0.8	83%
Congo River & estuary															
Congo @ Linda	S5207	97.8	130	3516	75	85	1	2.2	1.8	4.2	2.4	2.2	2.1	1.1	47%
Congo @ Brazzaville	S3533	98.5	70	6547	63	72	1	1.0	1.4	3.9	0.7	0.7	1.1	0.3	44%
Congo @ Kinshasa	S5114	96.9	497	911	85	90	1	3.2	4.4	12.2	2.6	2.2	4.1	1.2	85%
Congo @ Isle de Mateba	S5115	97.6	57	7989	76	87	1	4.0	2.2	8.1	2.1	1.9	3.4	1.1	41%
Estuary channel @ Soyo	S4899	96.6	86	5236	90	94	1	5.6	4.6	12.8	7.3	6.9	4.3	2.8	36%
Estuary beach @ Soyo	S4898	96.2	42	10,651	73	77	3	4.2	4.4	2.9	1.3	2.0	1.6	0.6	23%
Atlantic coast															
Libreville beach	S5530	93.8	33	13,410	35	57	14	1.5	0.4	4.7	0.3	0.7	0.4	0.2	66%
Pointe Noire beach	S0162	98.2	26	17,393	60	90	1	3.7	0.6	22.5	2.4	3.0	0.8	0.7	51%
Loussoni River	S4053	98.3	80	5767	80	82	0	2.1	2.3	6.3	1.4	1.1	1.4	0.5	53%
Loémé River	S0161	99.0	203	2286	96	90	0	1.3	2.2	8.0	3.4	2.7	1.9	1.1	64%
Quifuma beach	S4902	94.9	48	9262	42	72	7	2.7	0.4	1.8	1.2	2.3	0.5	0.4	20%
Luculu river mouth	S4904	91.9	439	978	62	74	11	3.2	1.6	2.2	1.3	2.7	1.0	0.6	46%
Mbua-Moyo beach	S4905	89.0	174	2394	41	67	18	2.2	0.4	1.2	1.2	2.4	0.4	0.5	67%

The Malagarasi River, sourced in southern Burundi, drains Mesoproterozoic to Neoproterozoic clastic rocks with intercalated mid-Neoproterozoic flood basalts, and the southwestern part of the Tanzania craton. Sand entering Lake Tanganyika is litho-quartzose with mafic volcanic and siltstone/sandstone rock fragments. The very poor tHM suite includes epidote, amphibole, andalusite, zircon, tourmaline, and minor rutile, staurolite and prismatic sillimanite.

In Rusizi and Malagarasi sand, SiO_2 is high (85–88 wt%), the CIA is 60–61, and α^{Al} indices for Sr, Ca, and Na mainly range between 2 and 3 (Table 2). Zr is ~100 ppm and the Eu anomaly moderately negative (Eu/Eu* 0.69–0.79).

4.2. Bas-Congo tributaries

Tributaries in the lower Congo course have variable composition (Figs. 7 and 8). Sand carried by the Nsele River, entering the Malebo Pool northeast of Kinshasa and draining Mesozoic and Cenozoic sediment covers of the *cuvette centrale*, is pure quartzose with a very poor tHM suite dominated by zircon, tourmaline and rutile, with minor staurolite and kyanite (Table 1). The U−Pb age spectrum of detrital zircon is multimodal, with Pan-African (27%) and Seke-Banza (15%) peaks, Eburnean (10%) and Neoarchean (6%) clusters, and rare Permian and Triassic grains (2%).

Sand carried by tributaries draining sedimentary to low-rank metasedimentary rocks of the Cataractes Group or the unconformably overlying Inkisi siliciclastic rocks range from pure quartzose (Inkisi; Fig. 7B) and quartzose (Lunkunga) to litho-quartzose (Kwilu; Fig. 7C) and quartzo-lithic metasedimentaclastic (Mbangala; Fig. 7D). Transparent-heavy-mineral suites range from poor and kyanite-dominated with minor garnet and staurolite (Inkisi) to very poor and either ZTR-dominated with anatase and rare monazite (Lunkunga, Kwilu), or tourmaline-dominated (Mbangala).

The U−Pb zircon-age spectra of Inkisi and Lunkunga sands are multimodal, with Pan-African (20% and 18%) and latest Mesoproterozoic (24%) peaks, and minor Eburnean (9% and 7%), and Neoarchean (6% and 4%) clusters. Inkisi sand also displays a Permo-Triassic (Karoo) cluster (5%; Fig. 9).

Tributaries of the lowermost course draining granitoid, metavolcanic, and metasedimentary rocks of the Seke-Banza Group together with the underlying Kimezian basement carry either quartz-rich feldspatho-quartzose sand with a rich epidote-dominated tHM suite including actinolite (Bundi), or litho-feldspatho-quartzose sand with a moderately rich tHM suite including epidote, amphibole, and zircon (Mpozo). U−Pb age spectra of detrital zircons are bimodal with a major Seke-Banza peak and a subordinate Eburnean cluster (15–22%). Bundi sand is characterized by a sharp peak at 906 ± 16 Ma, suggesting massive provenance of zircon grains from igneous rocks of the Seke-Banza Group (Fig. 6). Mpozo sand displays a slightly older peak (962 ± 26 Ma) and also includes a minor early Mesoproterozoic cluster (~1.48 Ga; 4%) and various early Paleoproterozoic to Mesoarchean ages.

Quartz enrichment is much stronger in Inkisi and Lunkunga sands (SiO_2 97–98 wt%) than in Mbangala, Bundi, and Mpozo sands (SiO_2 84–90 wt%). The CIA decreases from as high as 87 for Inkisi sand to 49–54 for Bundi and Mpozo sand (Table 2). Zr is 100–150 ppm in Inkisi, Lunkunga, and Mbangala sands but reaches 300–400 ppm in Bundi and Mpozo sands. REEs are highest in Mbangala sand and the Eu anomaly ranges from 0.44 in Lunkunga sand to 0.89 in Bundi sand.

4.3. Congo River

Congo River sand in Bas-Congo is pure quartzose (Fig. 7A, F), with mainly well rounded to subrounded monocrystalline quartz commonly displaying abraded overgrowths (Qp/Q < 5%), few feldspars, negligible lithic fragments, and very poor tHM suites dominated by zircon, tourmaline, and rutile. Upstream of Malebo Pool, altered plagioclase or K-feldspar grains, and granitoid, felsic volcanic, quartzose siltstone, or chert rock fragments are only rarely recorded; staurolite, minor epidote, sillimanite, kyanite, anatase, amphibole, augitic clinopyroxene, and rare andalusite and Cr-spinel occur. Between Kinshasa and Matadi,

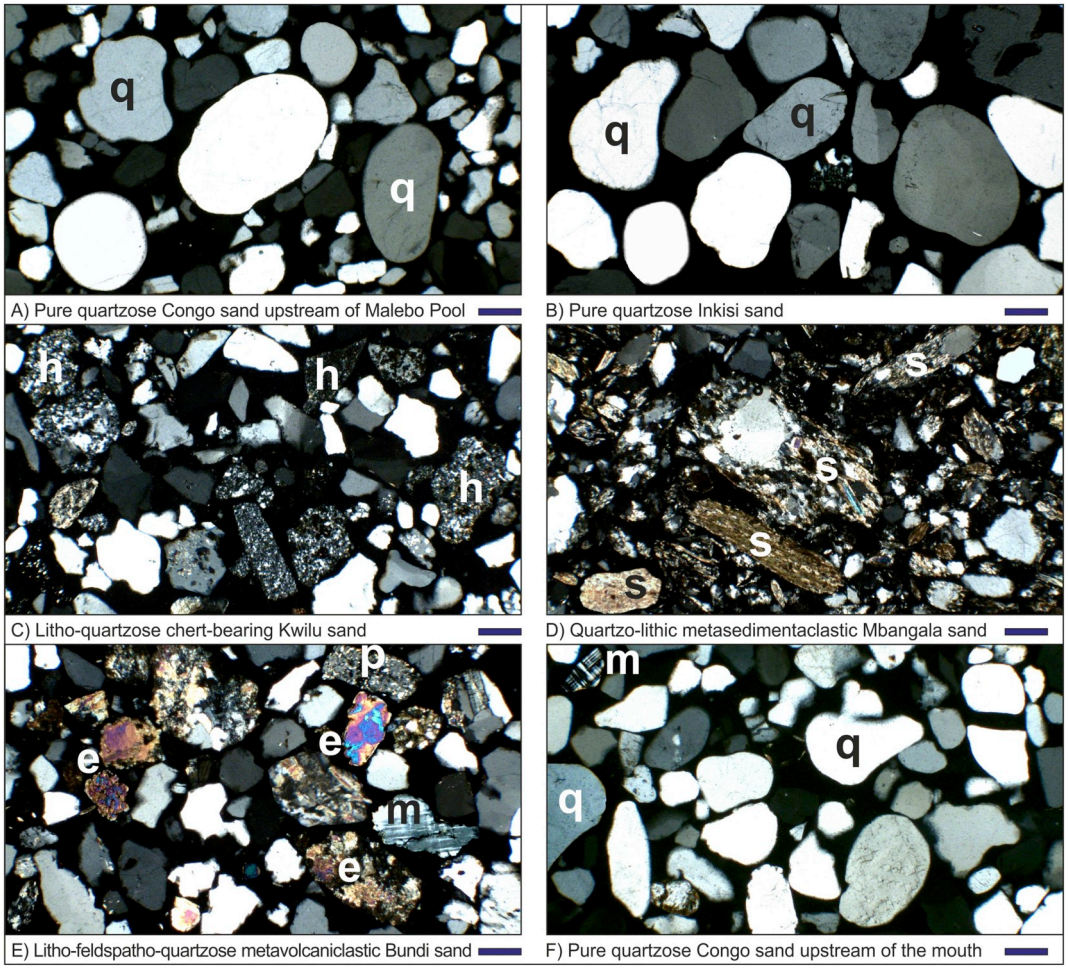

Fig. 7. Petrography of river sand in Bas-Congo. (A) Monocrystalline quartz grains, almost the sole survivors to intense weathering and multiple recycling in the *cuvette centrale*. Note that quartz roundness increases with grain size. (B) Rounded monocrystalline quartz multiply recycled from Neoproterozoic to Mesozoic sandstones in Bas-Congo. (C, D) Sand shed from sedimentary and very-low-grade metasedimentary rocks of the Cataractes Group. (E) Sand largely derived from metavolcanic rocks of the Seke-Banza Group. (F) Congo sand downstream of Boma, still dominantly consisting of monocrystalline quartz. Abbreviations: e = epidote; h = chert; m = cross-hatched microcline; p = plagioclase; q = quartz; s = shale/slate and other pelite to low-rank-metapelite lithics. Blue scale bar for scale = 100 μm. (For interpretation of the references to colour in this figure legend, the reader is referred to the web version of this article.)

Congo sand contains a little more polycrystalline quartz, feldspars (P/F 13–43%), metasedimentary rock fragments, and muscovite, together with a little more epidote, amphibole, garnet, and kyanite. Estuary sand downstream of Boma (P/F 40–57%) has lower ZTR index and relatively higher epidote, tourmaline, amphibole, and kyanite (Table 1).

The multimodal U–Pb zircon-age distribution in trunk-river sand across Bas-Congo includes: (1) a few Permo-Triassic grains; (2) a major Pan-African peak around 0.6 Ga, decreasing from ~27% upstream of Malebo Pool to ~21% in estuary sand; (3) a subordinate peak around 1.0 Ga, rather constant from ~19% upstream of the Malebo Pool to ~18% in the estuary); (4) an Eburnean cluster (~12%); (5) a Neoarchean cluster (~7%) (Fig. 9).

Prominent quartz enrichment in river and estuary sand is reflected in very high SiO_2 (96–98 wt%), with minor Al_2O_3 (< 1.5 wt%), Fe_2O_3 (< 0.6 wt%) and TiO_2 (< 0.5 wt%), and low trace-element concentrations (Zr mainly 42–86 ppm, Ba mainly 26–38 ppm). Chemical weathering indices are notably variable and high but not extreme (CIA 63–90, CIX 72–94), whereas the WIP is mostly 1 only. Alpha indices referred to Al are highest for Na, and mostly < 5 for Mg, Ca and Sr, ~2 for K and Rb, and ≥ 1 for Ba (Table 2). In estuary mud, far less affected by quartz enrichment (SiO_2 46 wt%), the CIA is 81, the CIX 91, the WIP 16, and α^{Al} indices reach 13 for Na and range between 3.7 and 3.0 for Mg, Sr, K, and Ca. Chondrite-normalized REE patterns display classical LREE enrichment (La_N/Sm_N 3–6 for sand, 4.1 for mud) and Eu anomaly generally more negative for sand than for mud (Eu/Eu* 0.46–0.69 vs. 0.66), suggesting monazite contribution. The lesser decrease for MREEs (Gd_N/Ho_N 0.8–1.7 for sand vs. 1.5 for mud) may reflect apatite contribution, whereas HREE distribution is flat to rising for sand (Gd_N/Yb_N 0.5–1.4 for sand vs.1.6 for mud), suggesting zircon contribution.

4.4. Atlantic coast south of the Congo mouth

Beach sand in northernmost Angola is pure quartzose, with poor to moderately poor tHM suites including epidote, amphibole, kyanite, garnet, and staurolite. The ZTR index steadily decreases southward from 13 to 3 (Table 1). Feldspar increases progressively southward (P/F 31–53%), and sand is quartzose south of the Luculu mouth, where tHM suites are moderately rich and include epidote, garnet, amphibole, and kyanite.

In beach sand ~20 km south of the Congo mouth, U–Pb zircon-age spectra are multimodal and similar to Congo estuary sand, with Pan-African (26%), Seke-Banza (15%), a larger Eburnean (20%), and Neoarchean (9%) clusters. The Eburnean cluster increases farther south (~47%) to become predominant along most of coastal Angola (Fig. 5 in Garzanti et al., 2018a). Triassic to Permian ages also tend to increase southward, reaching 9% in Luculu mouth sand.

Geochemical composition reflects mineralogical composition, with progressive southward decrease in SiO_2 from 95 to 89 wt% and

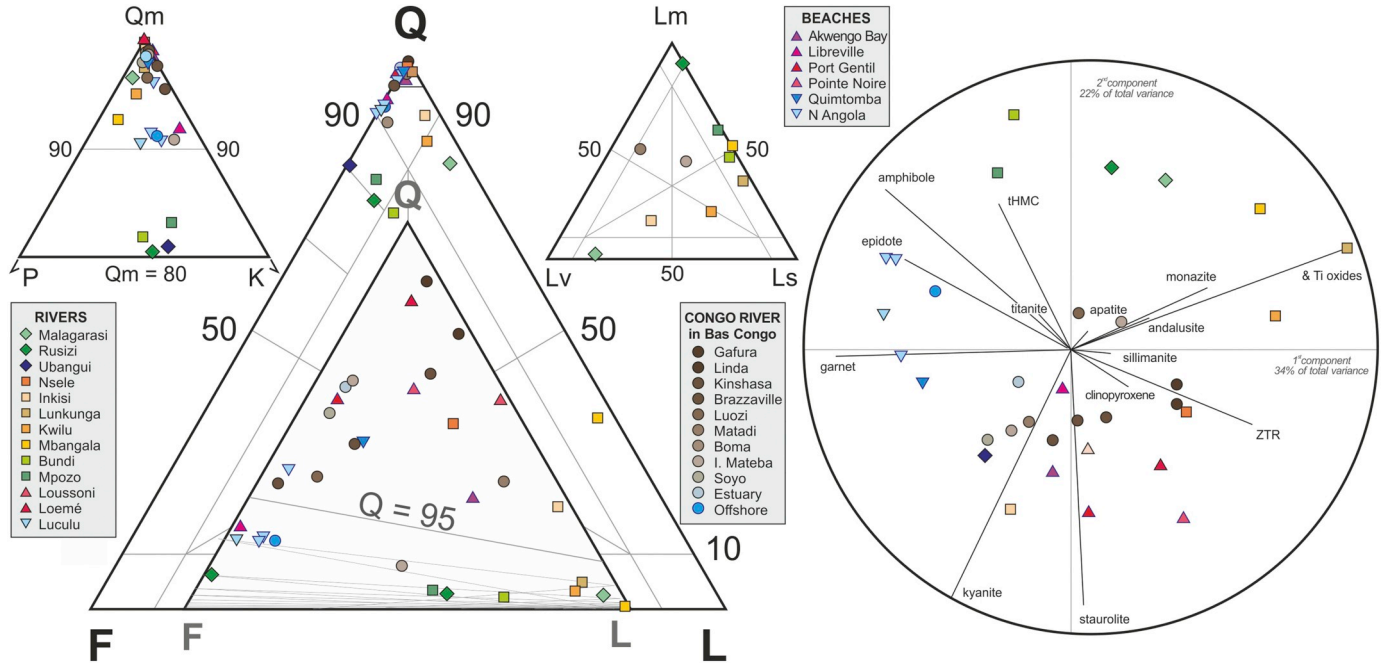

Fig. 8. Petrography and heavy minerals. Pure quartzose composition and ZTR-dominated tHM suites characterize Congo sand upstream of Malebo Pool and coastal sand north of the mouth, whereas sand of Congo tributaries in the upper catchment and in Bas-Congo, sand of coastal Angola, and offshore muds include less durable minerals in various proportions. Q = quartz (Qm = monocrystalline); F = feldspars (P = plagioclase; K = K-feldspar); L = lithics (Lm = metamorphic; Lv = volcanic; Ls = sedimentary); ZTR = zircon + tourmaline + rutile; tHMC = transparent-heavy-mineral concentration. Fields in the QFL diagram after Garzanti (2019); in the nested version of the same QFL plot, data are centered to allow better visualization of pure quartzose samples (von Eynatten et al., 2002; Comas-Cufí and Thió-Henestrosa, 2011). In the compositional biplot (Gabriel, 1971), both multivariate observations (points) and variables (rays) are displayed. The length of each ray is proportional to the variance of the corresponding element in the data set. If the angle between two rays is close to 0°, 90°, or 180°, then the corresponding elements are directly correlated, uncorrelated, or inversely correlated, respectively.

consequent weaker dilution of most other elements. Chemical indices indicate lower weathering than in Congo sand (Table 2). Luculu mouth mud, however, yielded very high values of weathering indices (CIA 90, CIX 94, WIP 9, α^{Al}Na 30). REE patterns become less steep and the Eu anomaly less negative southward (La_N/Sm_N 5–7 vs. 9.3; Eu/Eu* 0.73–0.81 vs. 0.68).

4.5. Atlantic coast north of the Congo mouth

Beach sand in the Republic of Congo is pure quartzose, consisting almost entirely of commonly rounded monocrystalline quartz grains displaying deep etch pits, with only a few microcline grains and a very poor tHM suite with zircon, rutile, tourmaline, staurolite, kyanite, and rare andalusite. River sand contains a few quartzose siltstone grains and very poor tHM suites dominated by zircon and tourmaline, with rutile, staurolite, kyanite, epidote, and garnet (Table 1). Chemical composition is almost pure SiO_2 (98–99 wt%). The CIA, CIX and α^{Al} indices are similar to those of Congo sand, and the WIP index is < 1. REE patterns are very steep (La_N/Sm_N 10.9–11.8) where zircon is rare (Zr 26–80 ppm), or nearly flat (La_N/Sm_N 1.3) where zircon occurs (Zr 203 ppm); Eu/Eu* is 0.50–0.66.

Medium to coarse-grained beach sand in Gabon is pure quartzose. Fine-grained beach sand is quartzose with mostly K-feldspar, and therefore characterized by lower SiO_2 and weathering indices than in the Republic of Congo. The very poor tHM suites are dominated by ZTR minerals with minor garnet, staurolite, amphibole, kyanite, and rare apatite, epidote and pyroxene (Table 2).

4.6. Shelf and deep-sea

Fine-grained sand collected on the inner shelf just south of the Congo mouth at 31 m b.s.l. is quartzose and includes common brown goethite ooids, a few plagioclase and K-feldspar grains (P/F 0.38), and a moderately rich tHM suite including epidote, garnet, amphibole, zircon, rutile, kyanite, and minor andalusite, tourmaline, apatite and staurolite. Very fine-grained shelfal sediment collected north of the Congo mouth at 45 m b.s.l. dominantly consists of brown pellets and foraminifera.

Deep-sea sediment cored offshore of the Congo mouth at 2400 to 3000 m b.s.l. contains fine silt (≤ 10 μm in mean diameter) notably richer in feldspar than Congo river and estuary sand. South of the Congo Canyon, sand-sized green glaucony grains with pellets, clay aggregates, bioclasts, and pyrite are dominant. The silt-sized feldspatho-quartzose siliciclastic fraction accounts for only < 2% of framework grains and includes quartz, albite, K-feldspar, and Ca-plagioclase (Q/F 2.3–3.1; P/F 0.67). Muscovite was rarely recorded. The very poor but notably varied tHM suite consists of epidote, hypersthene, clinopyroxene, amphibole (including rare oxy-hornblende), minor zircon, apatite, tourmaline, and rare kyanite, sillimanite, enstatite and olivine (Table 1).

North of the Congo Canyon, sediment mostly consists of bioclasts or pellets and clay aggregates with glaucony and pyrite. The silt-sized feldspatho-quartzose siliciclastic fraction, accounting for 4–6% of framework grains, includes quartz and Ca-plagioclase dominating over albite and K-feldspar (Q/F 2.1–2.8; P/F 0.83–1.00). Muscovite was rarely recorded. The very poor tHM suite is dominated by green augite and hypersthene, with subordinate amphibole (dominantly oxy-hornblende but including even rare glaucophane), minor zircon and epidote, and rare rutile, garnet, tourmaline, corundum and olivine.

Because shelfal to deep-marine sediments are typically dominated by intrabasinal and authigenic grains including bioclasts, glaucony, ferruginous ooids or pyrite (Giresse, 1980), their chemical composition can be hardly compared with that of siliciclastic fluvial and beach sands, which dominantly consist of quartz, feldspar, and other extrabasinal detrital minerals. SiO_2 accounts for < 50 wt% and Al_2O_3 is ~15 wt% in deep-sea muds, which tend to have higher K, Rb, Pb, Mg, Mn, Ni, and Cu, and lower Ca, Sr, Zr, Ti, and Zn than mud at the Congo

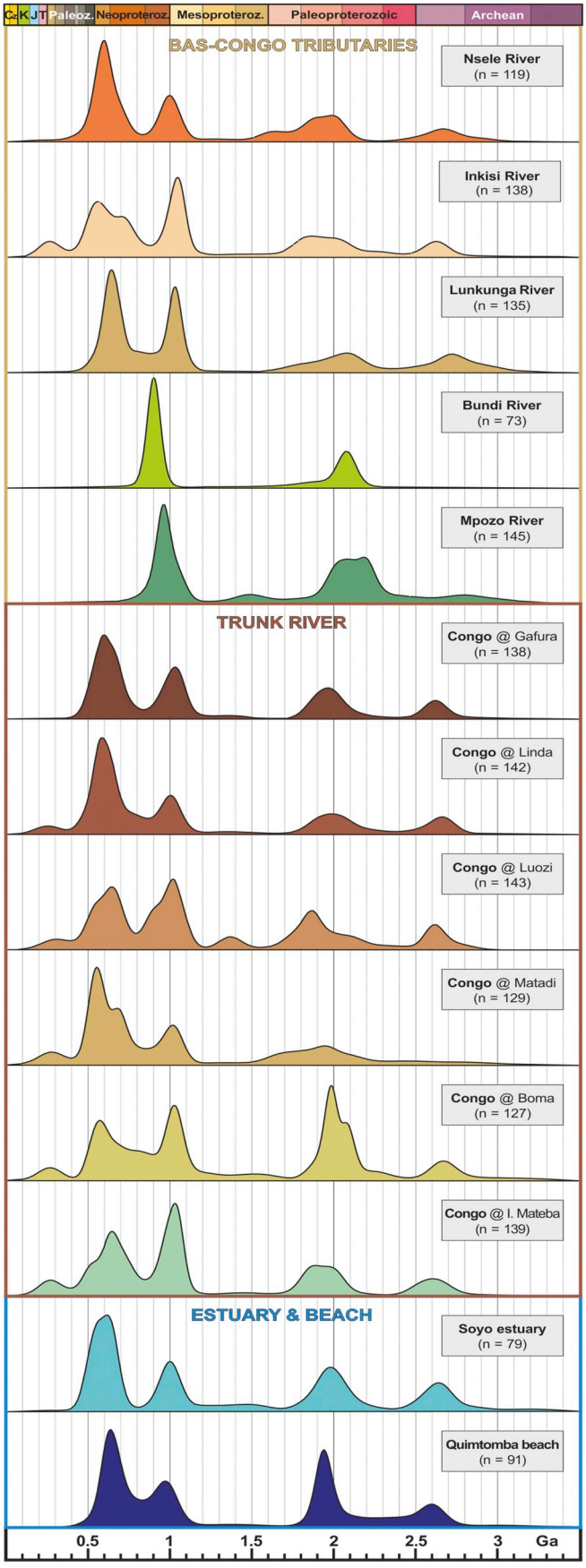

Fig. 9. U–Pb ages of detrital zircons (age vs. frequencies plotted as Kernel Density Estimates using the *provenance* package of Vermeesch et al., 2016). Congo sand is characterized by polymodal spectra with four major age clusters at ~0.6, ~1.0, ~2.0, ~2.6 Ga, and a few Permo-Triassic and Mesoproterozoic ages. The same age clusters recur in eastern Bas-Congo tributaries draining the Cataractes Group and younger sedimentary rocks, whereas Bundi and Mpozo sands display a major Seke-Banza peak with subordinate Eburnean cluster.

or Luculu river mouths. Shelfal sand rich in goethite ooids has also SiO_2 < 50 wt% but it is much richer than fluvial and beach sand especially in Fe, but also in Mg, Mn, Rb, Ni, and Zn.

5. Provenance

Provenance inferences drawn in this section include the relative zircon budget and the origin of offshore sediments, which document contributions from sources other than the Congo River, including long-distance airborne transport from volcanic centres.

5.1. Hints from detrital zircon

The same multimodal zircon-age spectra observed in upper Mesozoic strata of the Kasai region (Agyemang et al., 2016) and in other regions of the vast Congo catchment (de Wit and Linol, 2015; Linol et al., 2016) are recorded in Congo River sand across Bas-Congo (Fig. 9). A similar multimodal spectrum characterizes sand of the Nsele tributary, mostly recycled from Mesozoic and Cenozoic sediments of the *cuvette centrale*.

Zircon-age spectra in sand of Bas-Congo tributaries draining the Atlantic Rise reflect those of zircon grains in parent rocks of the West Congo Supergroup and Kimezian basement (Frimmel et al., 2006; Affaton et al., 2016). Pan-African, Seke-Banza, and minor Eburnean and Neoarchean clusters occur in Lunkunga sand, where zircon grains are all recycled from siliciclastic rocks of the Cataractes Group (Fig. 6). Bundi and Mpozo sands, instead, are characterized by early Neoproterozoic (Tonian) and mid-Paleoproterozoic (Rhyacian-Orosirian) peaks, reflecting largely first-cycle supply from Seke-Banza igneous and metaigneous rocks and subordinate direct or indirect supply from Kimezian basement (Fig. 6C). Among tributaries joining the trunk river downstream of Malebo Pool, only the Inkisi carries a few Permo-Triassic zircons.

Most zircon grains carried by the Congo River to the ocean are polycyclic and reworked even several times from Neoproterozoic and younger siliciclastic rocks. Given the broad similarity of zircon-age spectra in trunk-river sand from upstream of Malebo Pool to the mouth, it is difficult to quantify the local supply from the Atlantic Rise relative to zircon grains derived from the *cuvette centrale* and upstream branches. The attempt illustrated in Fig. 10 suggests that local sources may account for a large proportion (up to 43%) of zircon grains reaching the estuary. Our integrated petrographic and heavy-mineral dataset indicates that zircon concentration is higher by an order of magnitude in sand of the Bundi and Mpozo tributaries draining igneous and metaigneous rocks of the Seke-Banza Group and underlying Kimezian basement than in trunk-river sand upstream of Malebo Pool (0.12–0.57% vs. 0.03–0.04% of framework grains). Based on these data, simple calculations suggest that Bas-Congo tributaries supply approximately 10% of total bedload reaching the Atlantic Ocean, where average zircon concentration has increased to 0.05–0.06%.

5.2. Offshore sediments

The siliciclastic fraction of sediments sampled at circalittoral to abyssal depths offshore of the Congo mouth is less quartz-rich and

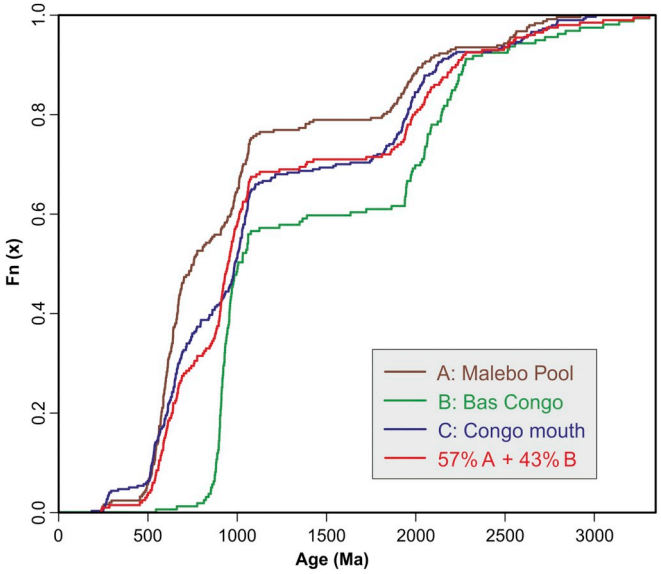

Fig. 10. Tentative estimate of zircon mixing proportions across Bas-Congo. Zircon U−Pb age data were amalgamated into group A (samples S5206 and S5207 from the Congo River upstream of Malebo Pool), group B (samples S5212 and S5213 from the Bundi and Mpozo tributaries), and group C (samples S4899, S5115, and S5215 from the trunk river at Boma and downstream). The least common multiple for the number of grains in A and B is $N = 39{,}273$. To create a synthetic mixture F (e.g., 23% of A with 77% of B), we combined F × N/n (A) copies of A with (100-F) × N/n (B) copies of B. We measured the Kolmogorov-Smirnov (KS) dissimilarity (Vermeesch, 2018b) between this synthetic mixture and sample C. Finally, the previous step was repeated for different mixing proportions until the KS dissimilarity was minimised. This occurred for F = 57% of A with 43% of B, with a bootstrapped confidence interval of +0.17/−0.18%.

distinct from Congo River sediments in both bulk mineralogy and heavy-mineral suites. Congo sand, therefore, is not distributed widely across the continental terrace but instead efficiently funnelled along the Congo Canyon to feed directly as turbidites the huge deep-sea fan. The extrabasinal fraction of fine-grained sand rich in brown goethite ooids collected on the inner shelf south of the mouth reflects contribution from northward longshore drift (Garzanti et al., 2018b). Instead, very fine sand north of the mouth consists of brown pellets and foraminifera entirely, indicating that longshore transport is interrupted at the Congo mouth, where northward-drifting sand is captured in the canyon and all conveyed to the deep sea.

The extrabasinal silt fraction contained in abyssal muds deposited both south and north of the Congo canyon includes Ca-plagioclase and very poor tHM suites characterized by augitic clinopyroxene and hypersthene locally associated with oxy-hornblende and olivine, indicating provenance from active volcanoes. Volcaniclastic detritus is more abundant in the north, and the source of ash fall is thus likely represented by the Cameroon Line - characterized by alkaline magmas mainly ranging in composition from olivine basalts to hypersthene-normative basalts - and most plausibly by its continental sector where explosive eruptions of trachytic to rhyolitic products are more frequent (Déruelle et al., 2007; Njome and de Wit, 2014).

6. Weathering and mineral durabilities

Notwithstanding the known limitations of weathering indices (Garzanti and Resentini, 2016 and references therein) and their imprecise determination in Congo sand because of extreme quartz enrichment and low content of all other elements including aluminium, the values obtained reflect extreme weathering conditions in the hot and hyper-humid equatorial Congo catchment (Négrel et al., 1993; Dupré et al., 1996). The CIA values calculated for Congo River sediments are in the same range as those obtained for Kagera River sediments derived from rift highlands in the east (CIA 63–90 vs. 71–87 for sand; CIA 81–91 vs. 77–88 for cohesive mud; Garzanti et al., 2013a, 2013b). The CIA values reach as high as 94–95 for Congo River clay, which dominantly consists of kaolinite (80–92% of clay minerals vs. 59–62% in Kagera mud). Weathering indices are not significantly different for sediments carried by Bas-Congo tributaries, where the CIA is 83–92 for cohesive mud (< 32 μm) and 88–95 for clay (Dinis et al., 2019). The indicative order of bulk-sediment mobility as defined by α^{Al} indices is $Na \gg Ca > Sr \geq Mg > K \approx Rb \geq Ba$ for sand and $Na \gg Ca > Sr > Mg \approx K > Ba \geq Rb$ for mud, which is in agreement with what observed along equatorial rift highlands to the east (Garzanti et al., 2013a, 2013b).

6.1. Quartz

Congo sand is dominated by mainly rounded and well rounded monocrystalline quartz, although finer grains may be angular to subangular (Fig. 7A, B, F). Strongly corroded quartz grains with concave outlines and etch pits are only a minority (e.g., compare with Figs. 3B, D, and 4C in Garzanti et al., 2013a). As for silicates in general, quartz solubility is influenced by pH, being minimum at pH ~3 and very low at ordinary temperatures in the typical range of ground water (pH 2–8; Brady and Walther, 1990). This explains why quartz is the most durable common mineral under most natural conditions, and why it is concentrated in sediments by weathering, especially where chemical attack is cumulated through multiple sedimentary cycles as recurred in the Congo catchment since the Neoproterozoic. Quartz solubility, however, may increase with increasing density of lattice dislocation and presence of microfractures. Strained monocrystalline grains with undulose extinction or polycrystalline grains with sutured contacts may thus be less durable and selectively depleted relative to unstrained monocrystalline quartz (Blatt, 1967a; Basu, 1985).

In Bas-Congo tributaries, quartz varies markedly from as high as 99%QFL in Nsele sand and 98%QFL in Inkisi sand, where corrosion pits and concave outlines are relatively uncommon as in trunk river sand (Fig. 7B and Fig. 7A,F), to as low as 35%QFL in Mbangala sand (Fig. 7D), where even deeply etched “runiquartz” is observed. Quartz abundance thus chiefly reflects the abundance of quartzose sandstone in the catchment and recycling, rather than weathering intensity.

6.2. Feldspars

Among the few detrital feldspars in Congo sand, 59% are untwinned K-feldspar, 15% cross-hatched microcline, and 26% plagioclase. In Bas-Congo tributaries, instead, plagioclase is as abundant as K-feldspar and cross-hatched microcline uncommon. In beach and river sand of the Republic of Congo and Gabon, plagioclase drops to 12% and cross-hatched microcline rises to 37%. Although feldspar abundance and relative proportions among feldspar types largely depend on source rock lithologies, these figures are in agreement with the widely assumed order of durability of detrital feldspars and their ability to survive weathering and recycling (i.e., microcline > orthoclase > plagioclase; Fig. 1 in Blatt, 1967b; James et al., 1981; Velbel, 1993). Although under active leaching Na^+ emigration rate from plagioclase exceeds K^+ emigration rate from orthoclase, cases in which K-feldspar may weather faster than plagioclase as a function of microchemical environment have long been documented in mature soils (e.g., Todd, 1968; Basu, 1985; Hinkley, 1996).

6.3. Carbonate vs. chert grains

Sands carried by the Congo River and by all of its studied tributaries lack carbonate grains, although carbonate rocks are exposed extensively in the Atlantic Rise and in various parts of the Congo

catchment upstream (Delpomdor and Préat, 2015; Delpomdor et al., 2015). Carbonate rock fragments were thus potentially produced in Bas-Congo, but dissolved completely probably because of high pCO_2 levels either in soils or river waters (Stumm and Morgan, 1996: p. 188ff; Karim and Veizer, 2000). Conversely, chert grains eroded from chert-bearing layers intercalated within the several carbonate intervals of the Cataractes Group (Cailteux et al., 2015) are common in Kwilu sand (Fig. 7C). These observations highlight the high durability of chert grains and, conversely, the solubility of carbonate grains in hyper-humid climate.

6.4. Mafic detritus

Thick metabasalt and amphibolite of early Neoproterozoic (Tonian) age are exposed along the West Congo Belt from northernmost Angola to Gabon ("*Roches vertes de Gangila*" of Tack, 1979; Nemba Group of Djama et al., 2018). These rocks are drained extensively by the Bundi River in Bas-Congo (Fig. 6C), and partly by the Loemé River in the Republic of Congo (Fig. 6A). Bundi sand is in fact distinguished from all of the other studied sediments by their relatively high amount of plagioclase and occurrence of metabasite rock fragments (8% and 1% of framework grains respectively), and by the rich tHM suite consisting almost entirely of epidote (6% of framework grains) with minor actinolite and zircon. Chemical analyses, however, fail to reveal major supply from mafic rocks. Ti is relatively high and the Eu anomaly only mildly negative (Eu/Eu* 0.89), but elements such as Fe, Mg, Sc, V, Cr, and Ni all have concentrations less than half of UCC values. Metabasite detritus is negligible in Loemé sand, where epidote represents only 8% of the poor tHM suite. These observations suggest that mafic detritus is weathered selectively, but does not undergo complete breakdown, in soil profiles developed on the Atlantic Rise.

6.5. Heavy minerals

The durability of rock-forming minerals at the conditions met at the Earth's surface is classically considered to follow in reverse the order of crystallization from high-temperature melts indicated by the Bowen series (i.e., olivine < pyroxene < amphibole; biotite < muscovite; plagioclase < K-feldspar < quartz; Goldich, 1938; Lasaga, 1984). Although expected to decrease with increasing polymerization of silica tetrahedra from nesosilicates and inosilicates to phyllosilicates and tectosilicates, vulnerability to weathering may vary widely among silicates having the same degree of tetrahedral connectedness. Among nesosilicates, where there is no corner-sharing among silica tetrahedra, the durability series olivine < garnet < staurolite < kyanite < andalusite < sillimanite < zircon is determined by the increasing strength of chemical bonds between non-tetrahedral cations and structural oxygen (Velbel, 1999).

The tHM suite of Congo sand is dominated by durable zircon, tourmaline and rutile, and upstream of Malebo Pool no other transparent heavy mineral represents > 10 tHM%. In all of the studied sand samples, about one third of transparent heavy minerals are corroded but two-thirds appear as relatively unweathered, and deeply etched and skeletal grains are rare. Etched pits are best displayed in amphibole grains, where weathering develops preferentially along cleavage planes (Velbel, 2007). Corrosion is visible on ~50% of staurolite grains, on 40–45% of amphibole, garnet and epidote grains, on 25–35% of kyanite, pyroxene and andalusite grains, and on < 20% of tourmaline, zircon, and rutile grains. Possible reasons why these surviving heavy-mineral species display a relatively limited degree of surface corrosion are discussed in Section 7.4 below.

6.6. Zircon

Although zircon accounts for more than a third of the tHM suite in Congo sand, zirconium is less than half relative to the UCC standard in many analysed samples (Table 2). Zr concentration, however, varies over one full order of magnitude, being as high as 497 ppm in the Kinshasa sample having the same grain size (~2.5 ϕ) as the three lowermost-course and estuary samples where Zr is only 42–86 ppm. In trunk-river sand, which as a first approximation can be considered to have the same provenance through Bas-Congo, Zr concentration correlates quite well with the Z/(Z + T) ratio ($r = 0.95$, sign. Lev. 0.1%). This parameter is introduced here as an index of hydraulic sorting, being zircon (Z; 4.6–4.7 g/cm^3) much denser than almost equally durable tourmaline (T; 3.03–3.25 g/cm^3). We conclude that the Kinshasa sample, where the zircon/tourmaline ratio reaches 5.7 versus 1.9 ± 1.4 in the other 10 samples, represents a semiplacer lag enriched in zircon by selective removal of less-dense settling-equivalent grains (Komar, 2007; Garzanti et al., 2009).

Besides such local hydraulic-sorting effects, Zr concentration is typically very low in Congo sand (e.g., 68 ppm in Congo bedload downstream of the Ubangui confluence; table 5 in Dupré et al., 1996) as in quartz-rich sand generated along the western branch of the East African rift where weathering conditions are also extreme (Zr 17–135 ppm; Garzanti et al., 2013a: p. 572–573). Sand of equatorial Africa is thus characterized by high SiO_2 and low Zr. The Si/Zr ratio in Congo River sand is higher than in the UCC standard by factors mostly between 2 and 5 (3500–8000 vs. 1620; Table 2). Quartz, therefore, is proved to have resisted multiphase recycling and intense weathering in the hyper-humid climate of equatorial Africa far better than zircon.

Corrosion of zircon starting from weak points such as inclusions or zoning has long been observed to occur under strong alkaline leaching during development of mature lateritic soil profiles (Carroll, 1953). Weathering of zircon under acid pH conditions is documented to occur in lateritic soils of central Gabon, induced by either chloride of marine origin or organic acids (Colin et al., 1993). Old and U/Th-rich metamictic zircons ultimately derived from Archean shields and characterized by disoriented isolated silica tetrahedra and a hydrous component (Woodhead et al., 1991) may be particularly sensitive to selective weathering, as long documented by experimental studies (Ewing et al., 1982; Balan et al., 2001). This would explain why zircon grains yielding Archean U—Pb ages represent only 9% of total detrital zircon in Congo sand (Fig. 9) even though the *cuvette centrale* is surrounded by Archean shields (Fig. 5).

7. The equatorial quartz sand factory

It is exceedingly difficult (Aitchison, 1986) to understand whether a sand is strongly enriched in quartz because of extensive weathering and breakdown of less stable components such as feldspar or because of overwhelming enrichment in quartz grains recycled from quartzarenite source rocks (Johnsson et al., 1988: p. 275; Basu, 2017: pp. 13–14). The incongruent dissolution of feldspar in lateritic soils testifies to intense weathering, but the kaolinite-rich fraction thus produced is separated from sand bedload during fluvial transport, entrained in suspension, and eventually segregated in floodplain and lagoonal mud or winnowed offshore. Textural analysis can help to evaluate only grossly whether dissolution or recycling is the prevailing mechanism leading to quartz enrichment. Chemical data offer useful help, although chemical-weathering indices are also dependent on source-rock lithology, hydraulic sorting, and grain size. Moreover, their calculation becomes unrobust where the sand is nearly pure SiO_2 with all other elements reduced to very small amounts.

7.1. Where is pure quartzose sand generated?

The Rusizi and Malagarasi Rivers sourced from the western branch of the East African rift and the Ubangui River draining the Congo craton carry litho-quartzose or feldspatho-quartzose sands with amphibole, kyanite, and epidote (Fig. 8). Congo River sand just upstream of Malebo Pool, instead, is pure quartzose and consists almost entirely of

monocrystalline quartz and durable heavy minerals. Among Bas-Congo tributaries, pure quartzose sand is transported by the Nsele and Inkisi Rivers, whereas Mbangala sand is quartzo-lithic metasedimentaclastic, Bundi sand is litho-feldspatho-quartzose, and Mpozo sand quartz-rich feldspatho-quartzose (Table 1). Trunk-river sand in Bas-Congo is pure quartzose, but includes minor amounts of less durable components indicating that contribution from lower-course tributaries is significant. Forward mixing calculations (Garzanti et al., 2012) based both on the integrated petrographic and heavy-mineral dataset and on geochemical data are remarkably consistent with the estimate based on the age spectra of detrital zircons (Fig. 10), suggesting that between 7% and 14% of total Congo bedload fed into the Atlantic Ocean is generated in the Atlantic Rise of Bas-Congo.

In beaches and coastal rivers of northernmost Angola, less durable components increase steadily southward, from the estuary to ~20 km, ~40 km, and ≥ 70 km south of the mouth (Garzanti et al., 2018a). North of the mouth, pure quartzose composition characterizes beaches and coastal rivers of the Republic of Congo and Gabon, although fine-grained beach sand may be quartzose with common K-feldspar. Petrographic data are corroborated by chemical data, indicating notably lower SiO_2 in Rusizi and Malagarasi sands than in Congo sand just upstream of Malebo Pool. SiO_2 decreases slightly across Bas-Congo, and from the estuary to beaches and coastal rivers of northernmost Angola ~40 km and ≥ 70 km south of the mouth. SiO_2 content is very high in beaches and coastal rivers of the Republic of Congo and Gabon (Table 2).

Geomorphological and climatic conditions strong enough to effectively destroy all minerals excepting durable quartz, zircon, tourmaline and rutile, therefore, are not met in the northern and eastern peripheral parts of the huge Congo River catchment, including the northern divide with the Sahel-Saharan region and the western branch of the East African rift. They do not occur in Bas-Congo either, nor in the hinterland of coastal Angola to the south, but they are met in the *cuvette centrale* and along the equatorial Atlantic coast of Africa to the north. The "quartz factory" is thus confined to the central part of the Congo catchment and to equatorial regions where rainfall is most intense (Fig. 1B).

7.2. How is pure quartzose sand generated?

Vast amounts of pure quartzose sand are stored in the cratonic interiors of most low-latitude continents. Climatic conditions reigning at present do not necessarily exert a fundamental control, because examples include not only humid to hyper-humid regions of South America drained by the Orinoco, Amazon, Paranà and Uruguay Rivers (e.g., Johnsson et al., 1988; Fig. 6 in Garzanti, 2019) but also semiarid to hyper-arid regions of Africa and Arabia occupied by the Mega-Kalahari, Sahara, Great Nafud, and Rub' al Khali deserts (Muhs, 2004; Garzanti et al., 2014a, 2017b). Large reservoirs of pure quartzose sand were common also in the past, such as the vast area extending during the Cambro-Ordovician across northern Gondwana from Oman to Mauritania (Burke, 1999; Avigad et al., 2005) and in Laurentia as well (Dott, 2003). This has notably influenced the way of thinking of sedimentary petrographers, who have traditionally considered pure quartzose sand as the standard product of prolonged mechanical abrasion and/or chemical weathering on relatively stable continental blocks (orthoquartzite of Krynine, 1941; quartzarenite of Folk, 1980: p. 139; craton interior subprovenance of Dickinson, 1985). Moreover, it contributed to the general but fallacious belief that sand is destined to improve its "maturity" through time (Folk, 1951; Pettijohn, 1954; Hubert, 1962). We may speculate, as cognitive neuroscience suggests (Boyer, 2008; McCauley, 2011), that even such a sedimentological version of the purity myth (Garzanti, 2017) may be nurtured by security networks in our brain, that lead us to repel sources of impurity and contamination (Douglas, 2003; Mann, 2005; Lawson, 2012) and to indulge in the teleologic illusion that things are ultimately destined to attain perfection (Popper, 1994).

The thorny issue that despite several attempts has not been clarified thoroughly so far (Pettijohn et al., 1972: pp. 223–227; Dott, 2003) is whether purity can be achieved exclusively by weathering and in which climatic conditions. If not, then chemical attack during both weathering and diagenesis inherited and integrated through multiple sedimentary cycles is required. Krynine (1941: pp. 1915–1916) held that first-cycle quartzarenites enriched in rounded tourmaline and zircon are a typical product of "*prolonged and intense chemical decay in peneplaned regions*", when "*after passage through beach or dune stages deposition proceeds on flat surfaces*" at the *"beginning or end of a geosynclinal cycle*". Conversely, Suttner et al. (1981: p. 1235) concluded that "*only a rare, unique combination of extreme conditions of climate (tropical), relief (low), and sedimentation rate (slow) can give rise to first-cycle quartz arenites"* and thus *"that the bulk of ancient quartz arenite is multicycle in origin"*.

Franzinelli and Potter (1983), Potter and Franzinelli (1985) and Johnsson et al. (1991) documented the occurrence of quartz-rich sand in the Orinoco and Rio Negro catchments of subequatorial South America. Johnsson et al. (1988) ascribed their generation to intense and prolonged chemical weathering, either in the Andean retroarc basin where largely orogenic detritus is temporary stored or in lowland parts of the Guyana shield characterized by very low erosion and transport rates. First-cycle sand generated from the elevated Guyana shield where only Proterozoic granitoid gneisses are exposed, however, still contains significant amounts of polycrystalline quartz, feldspars, and rock fragments (Q84 F11 R5; Qp/Q 18%; P/F 14%; SiO_2 93 ± 1 wt%). Pure quartzose sand occurs only in catchments where cover strata including thick upper Proterozoic quartzarenite is exposed (Q97 F1 R2; Qp/Q 13%; P/F 88%; SiO_2 97 ± 2 wt%), and in the lowlands (Q99 F1 R0; Qp/Q 6%; P/F 7%; SiO_2 99 ± 4 wt%; data after tables 3 and 4 in Johnsson et al., 1991).

First-cycle sand generated entirely from granitoid or amphibolite-facies gneissic rocks exposed in rift highlands of subequatorial Africa contain more feldspar (up to 14%) and high-rank metamorphic lithics (up to 8%) than Congo sand does. Plagioclase is still present, although strongly depleted, and amphibole, sillimanite, staurolite, and andalusite are common whereas garnet is almost completely weathered out (Q/QFL 82–97%; Qp/Q 0–30%; Q/(Q + F) 81–99%; P/F 0–68%; ZTR 11–60; data after Garzanti et al., 2013a). Transformation of crystalline bedrock into a pure quartz sand is thus advanced but by no means carried out to completion, possibly not because of insufficiently intense or prolonged pedogenesis but because in high-relief areas subject to relatively rapid erosion fresher detritus may be contributed by landslides involving bedrock, fostered by concentrated rainfall during the rainy season.

7.3. How pure is pure?

The final answer about the possibility that pure quartzose sand or quartzarenite can be generated during a single sedimentary cycle … largely depends on the definition of quartzarenite! The conventional limits indicated for the quartzarenite field vary in fact notably in the literature, from wider (both feldspars and rock fragments < 10%QFR in Gilbert, 1954, Dott, 1964, and Johnsson et al., 1991; ≈ quartzose sand of Garzanti, 2019) to narrower (both feldspars and rock fragments < 5%QFR in Folk, 1954 and Franzinelli and Potter, 1983) and narrowest (Q > 95%QFR in Folk, 1980 and Dott, 2003; ≈ pure quartzose sand of Garzanti, 2019). Moreover, purity depends on grain size as well, medium and coarser-grained quartzarenites being commonly interlayered with finer-grained feldspatho-quartzose sandstones and siltstones (Odom et al., 1976; Dott, 2003: p. 390).

Many geological problems are blurred by semantic and scale issues, and this one is another example. Instead of "*are first-cycle quartzarenites possible?*" (Dott, 2003: p. 392) we may ask "*how quartz-rich can a sand shed entirely from granitoid or gneissic basement be?*". The problem is scale-dependent and must be tackled in small modern rivers ("first-

order sampling scale" of Ingersoll et al., 1993) draining granitoid or gneissic rocks exclusively (e.g., von Eynatten et al., 2016). The study of large rivers such as the Congo can provide an only qualitative, or at best semi-quantitative answer, because first-cycle and polycyclic detritus are invariably mixed in large proportions in huge catchments including vast lowland areas. Because quartz-rich sandstones have high sand-generation potential, their supply of recycled quartz grains may be relevant even where their exposure areas are relatively small and erosion rates moderate.

These lines of reasoning imply that no ancient quartzarenite can be safely considered as entirely first-cycle and exempt from recycling, because complete absence of quartz-rich siliciclastic cover strata in both highland and lowland parts of the sediment-routing system from source to sink is an unlikely assumption. As a consequence, inferences on paleoclimatic conditions leading to extensive weathering cannot be drawn, also because selective dissolution of unstable grains may be markedly enhanced after deposition during burial diagenesis (McBride, 1985).

Although surrounded by Archean shields and Proterozoic orogenic belts (Fig. 5), the Congo catchment hosts thick quartz-rich siliciclastic units of various ages, which have been exposed to multiple episodes of erosion and recycling throughout the Neoproterozoic (Frimmel et al., 2006; Tait et al., 2011), Paleozoic (Tack et al., 2008; Linol et al., 2015d), Mesozoic (Kadima et al., 2011; Agyemang et al., 2016), and Cenozoic (Giresse, 2005; Guillocheau et al., 2015). Recycling of largely Mesozoic and Cenozoic siliciclastic covers occurs extensively today all across the *cuvette centrale*.

In Bas-Congo, recycling of Neoproterozoic and Paleozoic sandstones fails to produce sand consisting exclusively of quartz and ZTR minerals. Only Inkisi sand is pure quartzose (Fig. 7B), but its tHM suite is kyanite-dominated. Although almost entirely recycled from the middle part of the Cataractes Group (Fig. 6), Mbangala sand is quartz-poor and dominated by low-rank metasedimentary lithic fragments (Fig. 7D). River and beach sands in the Republic of Congo to the north are largely derived from the same Neoproterozoic units (Affaton et al., 2016) and dominantly consist of quartz associated with ZTR minerals, but kyanite, staurolite, or even garnet still occur in minor amounts. In Gabon beaches, coarse sand is pure quartzose but fine-grained sand may contain common K-feldspar; although ZTR-dominated, tHM suites contain garnet, staurolite, and minor amphibole, kyanite, apatite, and epidote. Even a few clinopyroxene and orthopyroxene grains occur, probably part of airborne tephra derived from volcanic centers of the Cameroon Line.

The lesson that we learn here resonates with, and goes beyond the statement in Suttner et al. (1981: p. 1235). The extreme weathering conditions met in subequatorial climate, even in rift highlands of central Africa where erosion rates are moderately high (Garzanti et al., 2013a), do promote the generation of pure quartzose first-cycle sand. But even a combination of intense weathering and extensive recycling may not be enough to produce sand consisting of quartz and ZTR minerals exclusively, as observed in Bas Congo. Some feldspars (generally mostly K-feldspar including microcline), and a few rock fragments (e.g., chert, felsic volcanic, or metasedimentary types) or moderately durable heavy minerals (e.g., staurolite, kyanite; van Loon and Mange, 2007) still occur invariably. The abundance of ultra-pure quartzarenite in the rock record does not only require a certain amount of recycling, but strongly suggests that post-depositional dissolution must have played a decisive role in the final cleansing of all grains other than quartz and ZTR minerals (McBride, 1985; van Loon, 2009).

7.4. Textural evidence of weathering

Textural analysis can only provide qualitative and often ambiguous information to discriminate the effects of weathering versus recycling. Surface textures such as frosting and rounding may be caused by different processes, including chemical dissolution and eolian abrasion, and consequently quartz grains with rounded corners may be undecidedly indicative of desert environments, equatorial soil processes, or multicyclicity (Crook, 1968; Dott, 2003: p. 390; Resentini et al., 2018). Recycling is unmistakably indicated by the presence of quartz grains with abraded syntaxial overgrowths and siltstone/sandstone rock fragments, which according to Johnsson et al. (1988: p. 275) represent "*the only unambiguous criterion … of a multi-cycle origin for at least one component of a sand*". Conversely, quartz grains with embayments and etch pits or "runiquartz" with deep re-entrants infilled by clay interspersed with Fe and Al oxides characterize the extreme weathering conditions found in soils of hot-humid sub-equatorial highlands (Cleary and Conolly, 1972; Schulz and White, 1999; Figs. 3B, D, and 4C in Garzanti et al., 2013a; Fig. 7A–E in Garzanti et al., 2018a).

In the studied samples, strongly etched quartz grains are relatively rare and corrosion features on transparent heavy minerals remarkably less widespread than observed in equatorial highlands of the East African rift (Andò et al., 2012). Because annual temperatures and rainfall are similar, or even hotter and more intense in the Congo catchment, these observations are rather unexpected, and may be ascribed either to selective mechanical destruction of deeply etched and skeletal grains during long-distance fluvial transport or to dilution by only slightly weathered grains recycled from siliciclastic rocks deposited during drier periods.

7.5. Insights from clay minerals

Weathering in hot-humid subequatorial climate results in the efficient flushing of mobile elements from chemically unstable minerals contained in parent rocks, and in the concentration of residual kaolinite in laterite-type soils. Kaolinite is dominant (≥ 77% of the clay-mineral assemblage) in all of the studied rivers in Bas-Congo, and reaches 98% in Bundi mud despite the river drains wide exposures of Gangila metabasalt (Dinis et al., 2019). Kaolinite is also dominant in offshore samples, although illite and smectite are notably more abundant (kaolinite 52–76%, illite 6–23%, smectite 11–28%: Gingele, 1992; kaolinite 39–63%, illite 24–43%, smectite 9–16%: Dinis et al., 2019), confirming the influence of sediment sources other than the Congo River (van der Gaast and Jansen, 1984). A kaolinite content > 50% characterizes mud on the Atlantic Ocean floors from offshore northern Angola to the Gulf of Guinea, where fluvial contribution from intensely weathered regions of subequatorial Africa mixes with illite-rich dust blown by northeasterly trade winds from the Sahel (Petschick et al., 1996). Instead, smectite may be derived from degradation of volcanic ashes ejected from volcanic centers of the Cameroon Line.

7.6. Insights from chemical data

Chemical information greatly helps in the challenging attempt to discriminate the effect of physical versus chemical processes on the mineralogy of clastic sediments (Fig. 11). A useful criterion is provided by the ratio between two chemical indices such as the CIA and the WIP, which respond very differently to recycling (fig. 13 in Garzanti et al., 2013a). The CIA is unaffected by silica concentration and measures the degree of feldspar hydrolysis in granitoid rocks in situ, ranging from 50 where feldspars are unweathered to 100 where they are transformed into a pure kaolinite residue by complete leaching of mobile elements (Nesbitt and Young, 1982). Sediments however, are more complex mixtures than granite grus, and the CIA may range from as low as 20–30 in pure basaltclastic sand to as high as 65–80, even in the absence of weathering, in mud rich in illite and/or smectite or in slate sand (von Eynatten et al., 2012; Garzanti and Resentini, 2016). Instead, the WIP decreases steadily, even in the absence of weathering, by simple dilution of alkali and alkaline-earth elements where quartz is progressively added to the sediment. The relationships between the CIA and the WIP (Fig. 11B), and between the concentration of mobile alkali and alkaline-earth metals and silicon (Fig. 11C) or aluminium

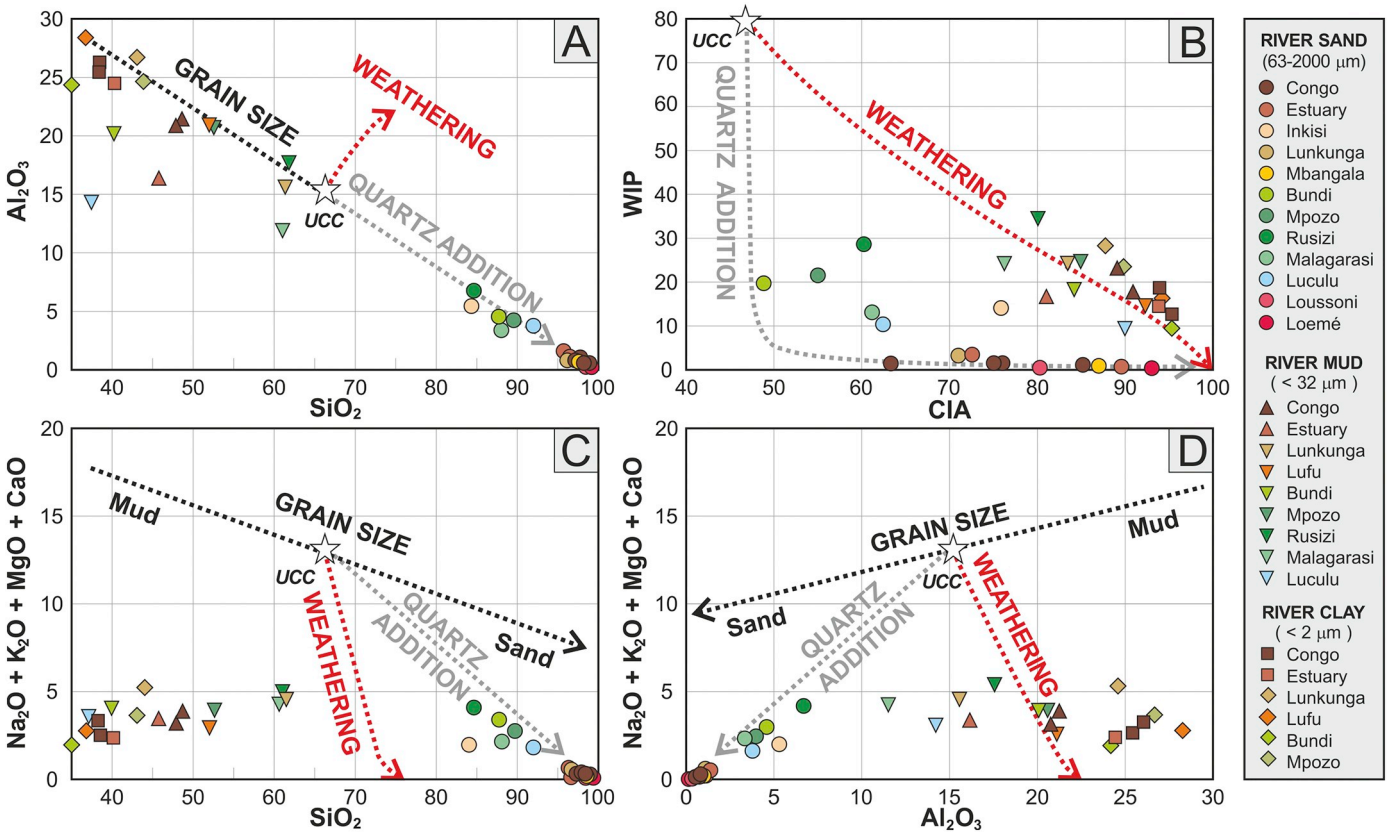

Fig. 11. Discriminating the effects of weathering, recycling, and grain size. Theoretical trends are all calculated starting from the Upper Continental Crust standard (UCC): the quartz-addition trend by progressively adding SiO_2, and the weathering trend by progressively subtracting mobile metals while assuming Si and Al as immobile. The grain-size trend is drawn parallel to empirical trends based on data from Alpine and Himalayan sediments (Garzanti et al., 2010, 2011, 2012). (A) The Al_2O_3/SiO_2 plot shows the superposed effects of grain size and quartz addition. Among samples plotting below the regression line ($Al_2O_3 = -0.45\ SiO_2 + 45$), Malagarasi sand and Bundi silt and clay are Fe-rich, reflecting occurrence of basaltic and metabasaltic source rocks. Luculu silt is also Fe-rich, whereas the Congo estuary silt sample has high LOI. (B) The CIA/WIP plot readily reveals quartz recycling, which affects strongly the WIP but not the CIA (Garzanti et al., 2013a, 2013b). In Congo sand, the CIA is unstable because of low Al_2O_3 and the WIP is invariably very low, documenting strong quartz addition. (C, D) Both plots show the dominant effect of weathering for mud and of quartz recycling for sand. Clay is affected only by weathering.

(Fig. 11D), highlight the effect of intense weathering for clay and silt, whereas the effect of recycling is overwhelming for sand. This confirms and expands on the observations made on sediments from Angola in the south (Dinis et al., 2017).

7.7. Unreliability of mineralogical indices of alteration

Chemical indices such as the CIA may provide misleading information on weathering conditions when applied to siliciclastic sediments. This is because the concentration of chemical elements in a sediment sample directly reflects its mineralogical composition, which depends primarily on several factors other than weathering, including provenance, grain size, and hydraulic sorting (e.g., Borges et al., 2008; Garzanti et al., 2010, 2011; von Eynatten et al., 2012, 2016). The existence of multiple controls on sediment mineralogy implies that mineralogical ratios are unreliable proxies for weathering intensity.

One emblematic example is the so called “Mineralogical Index of Alteration” MIA = Q/(Q + F)*100, based on the relative proportions between quartz and feldspar as determined by either X-ray diffraction (Rieu et al., 2007) or petrographic point-counts (Hessler et al., 2017). The Q/F ratio, a parameter long demonstrated to increase with sediment grain size (Odom et al., 1976; McBride et al., 1996; Sciunnach and Garzanti, 1996; Garzanti et al., 2003; Dott, 2003), can hardly be turned into an index of weathering by calling it “MIA”. The weakness of paleoclimate inferences drawn from such a parameter (e.g., Liivamägi et al., 2015; Hunger et al., 2018) is readily seen when the same maximum “MIA” value of ~100 characterizes modern fluvial sand generated in the hyper-humid Congo *cuvette* and dune sand accumulated in the hyper-arid Sahara and Arabian deserts (Muhs, 2004; Garzanti et al., 2013c). Climatic conditions cannot be determined directly by mineralogical parameters.

8. Conclusions

The Congo is the largest big river on Earth that carries pure quartzose sand to the ocean. Although difficult to access, its huge catchment provides an unexcelled setting in which to investigate the tectonic, geomorphological, climatic, and chemical conditions leading to the generation of pure quartzose sand. In this article we put to test the diverse criteria and available tools used to discriminate the relative effectiveness of weathering and recycling. The following conclusions are drawn:

1. modern river sands in the upper Congo catchment and in Bas-Congo are quartz-rich, but pure quartzose sand is generated only in the *cuvette centrale* (Fig. 8). Independent calculations based on the integrated petrographic/heavy-mineral dataset, on geochemical data, and on zircon-age spectra converge to suggest that between 7% and 14% of bedload supplied to the Atlantic Ocean is generated in Bas-Congo, reflecting rapid incision of river channels into the recently uplifted Atlantic Rise (Fig. 4);
2. quartz is enriched relative to all other minerals including zircon, probably because U-rich zircon grains derived from old Archean cratons have been selectively weathered out during successive

sedimentary cycles, as suggested by their low percentage in modern Congo sand (Fig. 9);
3. carbonate grains are absent in sands of the Congo River and of its Bas-Congo tributaries even where carbonate rocks are exposed, indicating complete dissolution either in soils or in river waters supersaturated with CO_2;
4. grain-surface textures convey ambiguous information. Quartz grains in Congo sand are mostly monocrystalline and largely well rounded (Fig. 7A,F), which may have resulted from weathering, recycling, or from a combination of both. Heavy-mineral suites are strongly depleted, which may be ascribed to either extensive weathering or recycling. The less durable surviving species only rarely appear to be strongly etched, which may hint either at mechanical destruction of skeletal grains during long-distance fluvial transport or at dilution by recycling of siliciclastic rocks deposited during drier periods in the past;
5. dominant kaolinite in Congo mud reflects extensive chemical weathering in the Congo catchment, whereas the mineralogy of offshore mud indicates mixing with wind-blown illite from the arid Sahel and with smectite derived from alteration of tephra probably ejected from volcanic centers of the Cameroon Line. Volcanic input is testified in abyssal mud cored at both sides of the Congo canyon by the presence of augitic clinopyroxene and orthopyroxene, locally associated with oxy-hornblende and olivine;
6. geochemical data on Congo mud, and especially on the clay fraction, reveal the prominent effect of weathering, which in Congo sand is masked by quartz recycling (Fig. 11);
7. mineralogical indices such as the so-called MIA = Q/(Q + F)*100 cannot be used as weathering indices because sediment mineralogy is controlled by several factors other than weathering, including provenance, grain size, and hydraulic sorting.

As general provenance implications and contributions to the everlasting debate on the origin of pure quartzose sand we conclude that:

1. no ancient quartzarenite can be safely considered as exempt from recycling, because no major sediment-routing system is likely to lack quartz-rich siliciclastic cover strata entirely from source to sink;
2. no ancient quartzarenite can be safely considered as produced by extensive weathering if selective dissolution of less stable grains during diagenesis cannot be ruled out;
3. first-cycle sand consisting of quartz and ZTR minerals exclusively cannot be generated by chemical weathering alone in the atmospheric and climatic conditions of the modern Earth;
4. the abundance in the rock record of sandstones consisting entirely of quartz and ZTR minerals cannot be satisfactorily explained by extensive chemical weathering, by physical recycling, or even by both combined. The complete breakdown of all other less stable minerals requires diagenetic dissolution, which operates at higher temperatures and over longer periods than weathering at the Earth's surface.

Acknowledgments

We heartily thank Giuditta Radeff, Marta Padoan, and Jasmine Petriglieri for their contribution in petrographic, heavy-mineral, and chemical analyses, Yixuan Li for assistance with the zircon U−Pb geochronology, Odhrán McCarthy for processing USGS DEM files, and François Guillocheau for providing publications. Massimo Dall'Asta, Attilio Schiavone, Maurizio Orlando, Daniela Dell'Era, Francesca Bolognesi, Hanna Haedke, and Hella Wittmann kindly helped us to obtain additional sand samples from Congo, D.R. Congo, and Gabon. Offshore sediment samples were provided by the GeoB Core Repository at MARUM – Center for Marine Environmental Sciences, University of Bremen (Germany). Funding was contributed by Project MIUR – Dipartimenti di Eccellenza 2018–2022, Department of Earth and Environmental Sciences, University of Milano-Bicocca. The manuscript benefited from careful constructive advice provided by Hilmar von Eynatten and Bernard Dennielou.

Appendix A. Supplementary data

Supplementary data associated with this article, to be found in the online version at https://doi.org/10.1016/j.jcorpfin.2019.07.014, include information on sampling sites (Table A1) together with the complete datasets on bulk-sand petrography (Table A2), heavy minerals (Table A3), surface textures (Table A4), sand geochemistry (Table A5), and detrital-zircon geochronology (Appendix B). The Google-Earth™ map of sampling sites Congo.kmz is also provided.

References

Affaton, P., Kalsbeek, F., Boudzoumou, F., Trompette, R., Thrane, K., Freie, R., 2016. The Pan-African West Congo belt in the Republic of Congo (Congo Brazzaville): Stratigraphy of the Mayombe and West Congo Supergroups studied by detrital zircon geochronology. Precambrian Res. 272, 185–202.

Agyemang, P.C.O., Roberts, E.M., Jelsma, H.A., 2016. Late Jurassic-Cretaceous fluvial evolution of Central Africa: Insights from the Kasai-Congo Basin, Democratic Republic Congo. Cretac. Res. 67, 25–43.

Aitchison, J., 1986. The Statistical Analysis of Compositional Data. Chapman and Hall, London, pp. 416.

Alsdorf, D., Beighley, E., Laraque, A., Lee, H., Tshimanga, R., O'Loughlin, F., Mahé, G., Dinga, B., Moukandi, G., Spencer, R.G.M., 2016. Opportunities for hydrologic research in the Congo Basin. Rev. Geophys. 54, 378–409.

Andò, S., Vignola, P., Garzanti, E., 2011. Raman counting: a new method to determine provenance of silt. Rend. Lincei Sci. Fis. Nat. 22, 327–347.

Andò, S., Garzanti, E., Padoan, M., Limonta, M., 2012. Corrosion of heavy minerals during weathering and diagenesis: A catalog for optical analysis. In: von Eynatten, H., Critelli, S., Ingersoll, R.V., Weltje, G.J. (Eds.), Actualistic Models of Sediment Generation. Sedimentary Geology, vol. 280. pp. 165–178.

Anka, Z., Séranne, M., Lopez, M., Scheck-Wenderoth, M., Savoye, B., 2009. The long-term evolution of the Congo deep-sea fan: a basin-wide view of the interaction between a giant submarine fan and a mature passive margin (ZaiAngo project). Tectonophysics 470, 42–56.

Anka, Z., Séranne, M., di Primio, R., 2010. Evidence of a large upper-Cretaceous depocentre across the Continent-Ocean boundary of the Congo-Angola basin. Implications for palaeo-drainage and potential ultra-deep source rocks. Mar. Pet. Geol. 27, 601–611.

Archibald, D., Glorie, S., Muanza-Kant, P., Baudet, D., Kanda-Nkula, V., Kitambala-Yaya, N., Mpiana-Kenababo, C., Nseka-Mbemba, P., Tack, L., 2018. The lower Diamictite Formation of the Cataractes Group, West Congo Supergroup (Bas-Congo region, DR Congo): A 678 my marker of extensional episodic activity during breakup of Columbia. In: 27th Colloqium of African Geology, 21/28 July 2018, Aveiro Portugal, pp. 29 Conference abstract.

Avigad, D., Sandler, A., Kolodner, K., Stern, R.J., McWilliams, M.O., Miller, N., Beyth, M., 2005. Mass-production of Cambro-Ordovician quartz-rich sandstone as a consequence of chemical weathering of Pan-African terranes: environmental implications. Earth Planet. Sci. Lett. 240, 818–826.

Azpiroz-Zabala, M., Cartigny, M.J., Talling, P.J., Parsons, D.R., Sumner, E.J., Clare, M.A., Simmons, S.M., Cooper, C., Pope, E.L., 2017. Newly recognized turbidity current structure can explain prolonged flushing of submarine canyons. Sci. Adv. 3, e1700200.

Babonneau, N., Savoye, B., Cremer, M., Klein, B., 2002. Morphology and architecture of the present canyon and channel system of the Zaire deep-sea fan. Mar. Geol. 19, 445–467.

Babonneau, N., Savoye, B., Cremer, M., Bez, M., 2010. Sedimentary architecture in meanders of a submarine channel: detailed study of the present Congo turbidite channel (Zaiango project). J. Sediment. Res. 80, 852–866.

Balan, E., Neuville, D.R., Trocellier, P., Fritsch, E., Muller, J.P., Calas, G., 2001. Metamictization and chemical durability of detrital zircon. Am. Mineral. 86, 1025–1033.

Basu, A., 1985. Influence of climate and relief on compositions of sands released at source areas. In: Zuffa, G.G. (Ed.), Provenance of Arenites. NATO ASI Series, vol. 148. pp. 1–18 Reidel, Dordrecht.

Basu, A., 2017. Evolution of siliciclastic provenance inquiries: a critical appraisal. In: Mazumder, R. (Ed.), Sediment Provenance, Influences on Compositional Change from Source to Sink. vol. 2. Elsevier, Amsterdam, pp. 5–23. https://doi.org/10.1016/B978-0-12-803386-9.00002-2.

Baudet, D., Tack, L., Fernandez-Alonso, M., Van den Haute, P., De Grave, J., Eeckout, S., Behiels, M., Kitambala-Yaya, N., Archibald, D.B., Glorie, S., 2018a. Detrital zircon geochronology and provenance analysis of the Matadi metaquartzites and Yelala metaconglomerates: Lithostratigraphic implications for the West Congo Supergroup (Bas-Congo region, DRC). In: 27th Colloqium of African Geology, 21/28 July 2018, Aveiro Portugal, pp. 68 Conference abstract.

Baudet, D., Kant-Kabalu, F., Nseka-Mbemba, P., Kadja-Wongudi, G., Mujinga-Mulamba, E., Phambu-Landu, J., Kanda-Nkula, V., Kitambala-Yaya, N., Muanza-Kant, P., Dewaele, S., Eekelers, K., Laghmouch, M., Theunissen, K., Tack, L., Fernandez-Alonso, M., 2018b. New 1/500.000 scale GIS-based geological and mineral resources

maps for Kongo Central province (DR Congo) with an updated lithostratigraphy of the West Congo Belt. In: 27th Colloqium of African Geology, 21/28 July 2018, Aveiro Portugal, pp. 64 Conference abstract.
Blatt, H., 1967a. Original characteristics of clastic quartz grains. J. Sediment. Petrol. 37, 401–424.
Blatt, H., 1967b. Provenance determinations and recycling of sediments. J. Sediment. Petrol. 37, 1031–1044.
Borges, J.B., Huh, Y., Moon, S., Noh, H., 2008. Provenance and weathering control on river bed sediments of the eastern Tibetan Plateau and the Russian Far East. Chem. Geol. 254, 52–72.
Boven, A., Theunissen, K., Sklyarov, E., Klerkx, J., Melnikov, A., Mruma, A., Punzalan, L., 1999. Timing of exhumation of a high-pressure mafic granulite terrane of the Paleoproterozoic Ubende belt (West Tanzania). Precambrian Res. 93, 119–137.
Boyer, P., 2008. Religion: Bound to believe? Nature 455, 1038–1039.
Brady, P.V., Walther, J.V., 1990. Kinetics of quartz dissolution at low temperatures. Chem. Geol. 82, 253–264.
Braga, E.S., Andrié, C., Bourès, B., Vangriesheim, A., Baurand, F., Chuchla, R., 2004. Congo River signature and deep circulation in the eastern Guinea Basin. Deep-Sea Res. I Oceanogr. Res. Pap. 51, 1057–1073.
Bultot, F., 1971. Atlas Climatique du Bassin Congolais. Publications de L'Institut National pour L'Etude Agronomique du Congo (I.N.E.A.C.). In: Deuxieme Partie, Les Composantes du Bilan d'Eau.
Burke, K., 1999. Tectonic significance of the accumulation of the voluminous early Paleozoic reservoir containing quartz-rich sandstones of North Africa and Arabia. Bull. Houst. Geol. Soc. 4, 11–13.
Cahen, L., Snelling, N.J., Delhal, J., Vail, J.R., Bonhomme, M., Ledent, D., 1984. Geochronology and Evolution of Africa. Oxford, Clarendon (512 pp).
Cailteux, J.L.H., Delpomdor, F.R.A., Ndobani, J.P.N., 2015. The Neoproterozoic West-Congo "Schisto-Calcaire" sedimentary succession from the Bas-Congo region (Democratic Republic of the Congo) in the frame of regional tentative correlations. Geol. Belg. 18 (2–4), 126–146.
Carroll, D., 1953. Weatherability of zircon. J. Sediment. Petrol. 23, 106–116.
CGMW-BRGM, 2016. In: Thiéblemont, D. (Ed.), Geological Map of Africa, 1:10 Million Scale, . www.brgm.fr.
Chandler, F.W., 1988. Quartz arenites: review and interpretation. Sediment. Geol. 58, 105–126.
Chew, D.M., Petrus, J.A., Kamber, B.S., 2014. U–Pb LA–ICPMS dating using accessory mineral standards with variable common Pb. Chem. Geol. 363, 185–199.
Cleary, W.J., Conolly, J.R., 1972. Embayed quartz grains in soils and their significance. J. Sediment. Petrol. 42, 899–904.
Colin, F., Alarcon, C., Vieillard, P., 1993. Zircon: an immobile index in soils? Chem. Geol. 107, 273–276.
Comas-Cufí, M., Thió-Henestrosa, F.S., 2011. CoDaPack 2.0: AStand-Alone, Multi-Platform Compositional Software.
Cramez, C., Jackson, M.P.A., 2000. Superposed deformation straddling the continental-oceanic transition in deep-water Angola. Mar. Pet. Geol. 17, 1095–1109.
Crook, K.A.W., 1968. Weathering and roundness of quartz sand grains. Sedimentology 11, 171–182.
De Grave, J., Van den Haute, P., Behiels, M., Eeckhout, S., Glorie, S., Archibald, D.B., Baudet, D., Fernandez-Alonso, M., Nseka Mbemba, P., Tack, L., 2018. Peralkaline granite bodies of the West Congo Belt (Matadi area, Bas-Congo region, DR Congo): Evidence of a 1.0 Ga lithospheric-scale extensional event during long-lived Columbia breakup. In: 27th Colloqium of African Geology, 21/28 July 2018, Aveiro Portugal, pp. 67 Conference abstract.
De Waele, B., Johnson, S.P., Pisarevsky, S.A., 2008. Palaeoproterozoic to Neoproterozoic growth and evolution of the eastern Congo Craton: its role in the Rodinia puzzle. Precambrian Res. 160, 127–141.
de Wit, M.J., Linol, B., 2015. Precambrian basement of the Congo Basin and its flanking terrains. In: de Wit, M.J., Guillocheau, F., de Wit, M.J.C. (Eds.), Geology and Resource Potential of the Congo Basin, Regional Geology Reviews. Springer-Verlag, Berlin Heidelberg, pp. 19–37.
Delaune, M., Jouanneau, J.M., Harle, J., Boulèque, J., 1995. Granulometrie et mineralogie des suspensions particulaires des fleuves Congo et Oubangui. In: Olivry, J.C. (Ed.), Grands bassins fluviaux périatlantiques; Congo, Niger, Amazone. ORSTOM, Paris, pp. 69–82.
Delpomdor, F., Préat, A., de Wit, M.J.C., 2015. Overview of the Neoproterozoic sedimentary series exposed along margins of the Congo Basin. In: de Wit, M.J., Guillocheau, F. (Eds.), Geology and Resource Potential of the Congo Basin, Regional Geology Reviews. Springer-Verlag, Berlin Heidelberg, pp. 41–58.
Delpomdor, F., Tack, L., Cailteux, J., Préat, A., 2015. The C2 and C3 formations of the Schisto-Calcaire Subgroup (West Congo Supergroup) in the Democratic Republic of the Congo: an example of post-Marinoan Sea-level fluctuations as a result of extensional tectonisms. J. Afr. Earth Sci. 110, 14–33.
Denamiel, C., Budgell, W.P., Toumi, R., 2013. The Congo River plume: Impact of the forcing on the far-field and near-field dynamics. J. Geophys. Res. Oceans 118, 964–989.
Dennielou, B., Droz, L., Babonneau, N., Jacq, C., Bonnel, C., Picot, M., Le Saout, M., Saout, Y., Bez, M., Savoye, B., Olu, K., Rabouille, C., 2017. Morphology, structure, composition and build-up processes of the active channel-mouth lobe complex of the Congo deep-sea fan with inputs from remotely operated underwater vehicle (ROV) multibeam and video surveys. Deep-Sea Res. II Top. Stud. Oceanogr. 142, 25–49.
Déruelle, B., Ngounouno, I., Demaiffe, D., 2007. The 'Cameroon Hot Line' (CHL): a unique example of active alkaline intraplate structure in both oceanic and continental lithospheres. C. R. Geosci. 339, 589–600.
Dickinson, W.R., 1985. Interpreting provenance relations from detrital modes of sandstones. In: Zuffa, G.G. (Ed.), Provenance of Arenites. Reidel, Dordrecht, NATO ASI Series, vol. 148. pp. 333–361.
Dinis, P., Garzanti, E., Vermeesch, P., Huvi, J., 2017. Climatic zonation and weathering control on sediment composition (Angola). Chem. Geol. 467, 110–121.
Dinis, P.A., Garzanti, E., Hahn, A., Vermeesch, P., Pinto, M.C., 2019. Weathering indices as climate proxies. A step forward based on Congo and SW African river muds. Earth Sci. Rev (This volume).
Djama, L.M.J., Bazika, U.V.M., Boudzoumou, F., Mouzeo, K., 2018. Petrology and geodynamic context of metabasic rocks of Nemba complex in the West Congo Fold Belt (Republic of Congo). Int. J. Geosci. 9, 1–18.
Dott, R.H., 1964. Wacke, graywacke and matrix – what approach to immature sandstone classification? J. Sediment. Petrol. 34, 625–632.
Dott, R.H., 2003. The importance of eolian abrasion in supermature quartz sandstones and the paradox of weathering on vegetation-free landscapes. J. Geol. 111, 387–405.
Douglas, M., 2003. Purity and Danger: An Analysis of Concepts of Pollution and Taboo. Routledge, Abingdon (UK), pp. 272.
Dupré, B., Gaillardet, J., Rousseau, D., Allègre, C.J., 1996. Major and trace elements of river-borne material: the Congo Basin. Geochim. Cosmochim. Acta 60, 1301–1321.
Eisma, D., Kalf, J., 1984. Dispersal of Zaire river suspended matter in the estuary and the Angola Basin. Neth. J. Sea Res. 17, 385–411.
Eisma, D., Kalf, J., van der Gaast, S.J., 1978. Suspended matter in the Zaire estuary and the adjacent Atlantic Ocean. Neth. J. Sea Res. 12, 382–406.
Ewing, R.C., Haaker, R.F., Lutze, W., 1982. Leachability of zircon as a function of alpha dose. In: Scientific Basis for Radioactive Waste Management. vol. 5. pp. 389–397.
Ferry, J.N., Babonneau, N., Mulder, T., Parize, O., Raillard, S., 2004. Morphogenesis of Congo submarine canyon and valley: implications about the theories of the canyons formation. Geodin. Acta 17 (4), 241–251.
Flint, J.J., 1974. Stream gradient as a function of order, magnitude, and discharge. Water Resour. Res. 10, 969–973.
Flügel, T.J., Eckardt, F.D., Cotteril, F.P.D., 2015. The present day drainage patterns of the Congo River system and their Neogene evolution. In: de Wit, M.J., Guillocheau, F., de Wit, M.J.C. (Eds.), Geology and Resource Potential of the Congo Basin, Regional Geology Reviews. Springer-Verlag, Berlin Heidelberg, pp. 315–337.
Folk, R.L., 1951. Stages of textural maturity in sedimentary rocks. J. Sediment. Petrol. 21, 127–130.
Folk, R.L., 1954. The distinction between grain size and mineral composition in sedimentary rock nomenclature. J. Geol. 62, 344–359.
Folk, R.L., 1980. Petrology of Sedimentary Rocks. Hemphill Publishing Co., Austin (USA), pp. 184.
Franssen, L., André, L., 1988. The Zadinian Group (late Proterozoic, Zaire) and its bearing on the origin of the West-Congo orogenic belt. Precambrian Res. 38, 215–234.
Franzinelli, E., Potter, P.E., 1983. Petrology, chemistry, and texture of modern river sands, Amazon River system. J. Geol. 91, 23–39.
Frimmel, H.E., Tack, L., Basei, M.S., Allen, P., Nutman, A.P., Boven, A., 2006. Provenance and chemostratigraphy of the Neoproterozoic West Congolian Group in the Democratic Republic of Congo. J. Afr. Earth Sci. 46, 221–239.
Furman, T., Graham, D., 1999. Erosion of lithospheric mantle beneath the East African Rift system: geochemical evidence from the Kivu volcanic province. Lithos 48, 237–262.
Gabriel, K.R., 1971. The biplot graphic display of matrices with application to principal component analysis. Biometrika 58, 453–467.
Gaillardet, J., Dupré, B., Allègre, C.J., 1999. Geochemistry of large river suspended sediments: silicate weathering or recycling tracer? Geochim. Cosmochim. Acta 63, 4037–4051.
Galehouse, J.S., 1971. Point counting. In: Carver, R.E. (Ed.), Procedures in Sedimentary Petrology. Wiley, New York, pp. 385–407.
Garzanti, E., 2017. The maturity myth in sedimentology and provenance analysis. J. Sediment. Res. 87, 353–365.
Garzanti, E., 2019. Petrographic classification of sand and sandstone. Earth Sci. Rev. 192, 545–563. https://doi.org/10.1016/j.earscirev.2018.12.014.
Garzanti, E., Andò, S., 2007. Heavy-mineral concentration in modern sands: Implications for provenance interpretation. In: Mange, M.A., Wright, D.T. (Eds.), Heavy Minerals in Use. Developments in Sedimentology, vol. 58. Elsevier, Amsterdam, pp. 517–545.
Garzanti, E., Andò, S., 2019. Heavy minerals for junior woodchucks. Minerals 9 (3), 148. https://doi.org/10.3390/min9030148.
Garzanti, E., Resentini, A., 2016. Provenance control on chemical indices of weathering (Taiwan river sands). Sediment. Geol. 336, 81–95.
Garzanti, E., Sciunnach, D., Confalonieri, M., 2003. Discriminating source rock and environmental control from detrital modes of Permo-Triassic fluvio-deltaic sandstones. I. Southern Alps (Lombardy, Italy). In: Valloni, V., Basu, A. (Eds.), Quantitative Provenance Studies in Italy. Memorie descrittive della Carta Geologica d'Italia, vol. 61. pp. 63–82.
Garzanti, E., Andò, S., Vezzoli, G., 2009. Grain-size dependence of sediment composition and environmental bias in provenance studies. Earth Planet. Sci. Lett. 277, 422–432.
Garzanti, E., Andò, S., France-Lanord, C., Vezzoli, G., Najman, Y., 2010. Mineralogical and chemical variability of fluvial sediments. 1. Bedload sand (Ganga-Brahmaputra, Bangladesh). Earth Planet. Sci. Lett. 299, 368–381.
Garzanti, E., Andò, S., France-Lanord, C., Galy, V., Censi, P., Vignola, P., 2011. Mineralogical and chemical variability of fluvial sediments. 2. Suspended-load silt (Ganga-Brahmaputra, Bangladesh). Earth Planet. Sci. Lett. 302, 107–120.
Garzanti, E., Resentini, A., Vezzoli, G., Andò, S., Malusà, M., Padoan, M., 2012. Forward compositional modelling of Alpine orogenic sediments. Sediment. Geol. 280, 149–164.
Garzanti, E., Padoan, M., Andò, S., Resentini, A., Vezzoli, G., Lustrino, M., 2013a. Weathering and relative durability of detrital minerals in equatorial climate: sand petrology and geochemistry in the East African Rift. J. Geol. 121, 547–580.
Garzanti, E., Padoan, M., Setti, M., Peruta, L., Najman, Y., Villa, I.M., 2013b. Weathering

geochemistry and Sr-Nd fingerprints of equatorial upper Nile and Congo muds. Geochem. Geophys. Geosyst. 14, 292–316.
Garzanti, E., Vermeesch, P., Andò, S., Vezzoli, G., Valagussa, M., Allen, K., Khadi, K.A., Al-Juboury, I.A., 2013c. Provenance and recycling of Arabian desert sand. Earth Sci. Rev. 120, 1–19.
Garzanti, E., Vermeesch, P., Padoan, M., Resentini, A., Vezzoli, G., Andò, S., 2014a. Provenance of passive-margin sand (Southern Africa). J. Geol. 122, 17–42.
Garzanti, E., Padoan, M., Setti, M., López-Galindo, A., Villa, I.M., 2014b. Provenance versus weathering control on the composition of tropical river mud (southern Africa). Chem. Geol. 366, 61–74.
Garzanti, E., Andò, S., Padoan, M., Vezzoli, G., El Kammar, A., 2015. The modern Nile sediment system: Processes and products. Quat. Sci. Rev. 130, 9–56.
Garzanti, E., Dinis, P., Vermeesch, P., Andò, S., Hahn, A., Huvi, J., Limonta, M., Padoan, M., Resentini, A., Rittner, M., Vezzoli, G., 2017a. Sedimentary processes controlling ultralong cells of littoral transport: placer formation and termination of the Orange sand highway in southern Angola. Sedimentology 65, 431–460.
Garzanti, E., Vermeesch, P., Al-Ramadan, K.A., Andò, S., Limonta, M., Rittner, M., Vezzoli, G., 2017b. Tracing transcontinental sand transport: from Anatolia-Zagros to the Rub' al Khali Sand Sea. J. Sediment. Res. 87, 1196–1213.
Garzanti, E., Dinis, P., Vermeesch, P., Andò, S., Hahn, A., Huvi, J., Limonta, M., Padoan, M., Resentini, A., Rittner, M., Vezzoli, G., 2018a. Dynamic uplift, recycling, and climate control on the petrology of passive-margin sand (Angola). Sediment. Geol. 375, 86–104.
Garzanti, E., Vermeesh, P., Rittner, M., Simmons, M., 2018b. The zircon story of the Nile: time-structure maps of source rocks and discontinuous propagation of detrital signals. Basin Res. 30, 1098–1117.
Gilbert, C.M., 1954. Sedimentary rocks. In: Williams, H., Turner, F.J., Gilbert, C.M. (Eds.), Petrography. Freeman, San Francisco, pp. 406.
Gingele, F., 1992. Zur klimaabhängigen Bildung biogener und terrigener Sedimente und ihrer Veränderung durch die Frühdiagenese im zentralen und östlichen Südatlantik. Doctoral dissertation, Berichte aus dem Fachbereich Geowissenschaften der Universität Bremen, 26. pp. 202.
Giresse, P., 1980. Carte sédimentologique du plateau continental du Congo. vol. 85. ORSTOM, Notice Explicative, Paris, pp. 33.
Giresse, P., 2005. Mesozoic–Cenozoic history of the Congo Basin. J. Afr. Earth Sci. 43, 301–315.
Goldich, S.S., 1938. A study in rock-weathering. J. Geol. 46, 17–58.
Goudie, A.S., 2005. The drainage of Africa since the Cretaceous. Geomorphology 67, 437–456.
Griffin, W.L., Powell, W.J., Pearson, N.J., O'Reilly, S.Y., 2008. GLITTER: Data reduction software for laser ablation ICP-MS. In: Sylvester, P. (Ed.), Laser Ablation-ICP-MS in the Earth Sciences: Current Practices and Outstanding Issues. 40. Mineralogical Association of Canada, pp. 204–207 Short Course Series.
Guillocheau, F., Chelalou, R., Linol, B., Dauteuil, O., Robin, C., Mvondo, F., Callec, Y., Colin, J.P., 2015. Cenozoic landscape evolution in and around the Congo Basin: constraints from sediments and planation surfaces. In: de Wit, M.J., Guillocheau, F., de Wit, M.J.C. (Eds.), Geology and Resource Potential of the Congo Basin, Regional Geology Reviews. Springer-Verlag, Berlin Heidelberg, pp. 271–313.
Guillocheau, F., Simon, B., Baby, G., Bessin, P., Robin, C., Dauteuil, O., 2018. Planation surfaces as a record of mantle dynamics: the case example of Africa. Gondwana Res. 53, 82–98.
Hack, J.T., 1957. Studies of longitudinal stream profiles in Virginia and Maryland. In: US Geological Survey Professional Paper 294-B. US Geological Survey, Reston (VA), pp. 45–97.
Heezen, B.C., Menzies, R.J., Schneider, E.D., Ewing, W.M., Granelli, N.C.L., 1964. Congo submarine Canyon. Am. Assoc. Pet. Geol. Bull., vol. 48, 1126–1149.
Hessler, A.M., Zhang, J., Covault, J., Ambrose, W., 2017. Continental weathering coupled to Paleogene climate changes in North America. Geology 45, 911–914.
Hinkley, T.K., 1996. Preferential weathering of potassium feldspar in mature soils. Am. Geophys. Union Geophys. Monogr. 95, 377–390.
Hoffman, P.F., Li, Z.X., 2009. A palaeogeographic context for Neoproterozoic glaciation. Palaeogeogr. Palaeoclimatol. Palaeoecol. 277, 158–172.
Hubert, J.F., 1962. A zircon–tourmaline–rutile maturity index and the interdependence of the composition of heavy mineral assemblages with the gross composition and texture of sandstones. J. Sediment. Petrol. 32, 440–450.
Hunger, G., Ventra, D., Moscariello, A., Veiga, G., Chiaradia, M., 2018. High-resolution compositional analysis of a fluvial-fan succession: the Miocene infill of the Cacheuta Basin (central Argentinian foreland). Sediment. Geol. 375, 268–288.
Ingersoll, R.V., Bullard, T.F., Ford, R.L., Grimm, J.P., Pickle, J.D., Sares, S.W., 1984. The effect of grain size on detrital modes: a test of the Gazzi-Dickinson point-counting method. J. Sediment. Petrol. 54, 103–116.
Ingersoll, R.V., Kretchmer, A.G., Valles, P.K., 1993. The effect of sampling scale on actualistic sandstone petrofacies. Sedimentology 40, 937–953.
Jackson, S.E., Pearson, N.J., Griffin, W.L., Belousova, E.A., 2004. The application of laser ablation-inductively coupled plasma-mass spectrometry to in situ U–Pb zircon geochronology. Chem. Geol. 211, 47–69.
James, W.C., Mack, G.H., Suttner, L.J., 1981. Relative alteration of microcline and sodic plagioclase in semi-arid and humid climates. J. Sediment. Petrol. 51, 151–164.
Johnsson, M.J., 1993. The system controlling the composition of clastic sediments. In: Johnsson, M.J., Basu, A. (Eds.), Processes Controlling the Composition of Clastic Sediments. Geological Society of America, Special Paper 284. pp. 1–19.
Johnsson, M.J., Stallard, R.F., Meade, R.H., 1988. First-cycle quartz arenites in the Orinoco River basin, Venezuela and Colombia. J. Geol. 96, 263–277.
Johnsson, M.J., Stallard, R.F., Lundberg, N., 1991. Controls on the composition of fluvial sands from a tropical weathering environment: sands of the Orinoco River drainage basin, Venezuela and Colombia. Geol. Soc. Am. Bull. 103, 1622–1647.
Kadima, E., Delvaux, D., Sebagenzi, S.N., Tack, L., Kabeyaz, S.M., 2011. Structure and geological history of the Congo Basin: an integrated interpretation of gravity, magnetic and reflection seismic data. Basin Res. 23, 499–527.
Karim, A., Veizer, J., 2000. Weathering processes in the Indus River Basin: implications from riverine carbon, sulfur, oxygen, and strontium isotopes. Chem. Geol. 170, 153–177.
Karner, G.D., Driscoll, N.W., 1999. Tectonic and stratigraphic development of the West African and eastern Brazilian margins: Insights from quantitative basin modelling. In: Cameron, N.R., Bate, R.H., Clure, V.S. (Eds.), The Oil and Gas Habitats of the South Atlantic. vol. 153. Geological Society, London, pp. 11–40 Special Publications.
Komar, P.D., 2007. The entrainment, transport and sorting of heavy minerals by waves and currents. In: Mange, M.A., Wright, D.T. (Eds.), Heavy Minerals in Use. Developments in Sedimentology Series. vol. 58. Elsevier, Amsterdam, pp. 3–48.
Kottek, M., Grieser, J., Beck, C., Rudolf, B., Rubel, F., 2006. World map of the Köppen-Geiger climate classification updated. Meteorol. Z. 15 (3), 259–263.
Krynine, P.D., 1941. Paleogeographic and tectonic significance of sedimentary quartzites. Geol. Soc. Am. Bull. 52, 1915–1916.
Laraque, A., Olivry, J.C., 1996. Evolution de l'hydrologie de Congo-Zaïre et de ses tributaires rive droite et dynamique de ses transports solides et dissous. L'hydrologie tropicale: géoscience et outil pour le développement (Proceedings from the Paris Conference, May 1995). IAHS Publ., no. 238. pp. 271–288.
Laraque, A., Bricquet, J.P., Olivry, J.C., Berthelot, M., 1995. Transports solides et dissous du fleuve Congo (bilan de six annees d'observations). In: Grands bassins fluviaux périatlantiques; Congo, Niger, Amazone. ORSTOM, Paris, pp. 133–145.
Laraque, A., Bricquet, J.P., Pandi, A., Olivry, J.C., 2009. A review of material transport by the Congo River and its tributaries. Hydrol. Process. 23, 3216–3224.
Laraque, A., Castellanos, B., Steiger, J., Lòpez, J.L., Pandi, A., Rodriguez, M., Rosales, J., Adèle, G., Perez, J., Lagane, C., 2013. A comparison of the suspended and dissolved matter dynamics of two large inter-tropical rivers draining into the Atlantic Ocean: the Congo and the Orinoco. Hydrol. Process. 27, 2153–2170.
Lasaga, A.C., 1984. Chemical kinetics of water-rock interactions. J. Geophys. Res. Solid Earth 89 (B6), 4009–4025.
Lavier, L.L., Steckler, M.S., Brigaud, F., 2001. Climatic and tectonic control on the Cenozoic evolution of the West African margin. Mar. Geol. 178, 63–80.
Lawson, E.T., 2012. Religious thought and behavior. Wiley Interdiscip. Rev. Cogn. Sci. 3, 525–532. https://doi.org/10.1002/wcs.1189.
Leturmy, P., Lucazeau, F., Brigaud, F., 2003. Dynamic interactions between the Gulf of Guinea passive margin and the Congo River drainage basin: 1. Morphology and mass balance. J. Geophys. Res. Solid Earth 108 (B8), 2383. https://doi.org/10.1029/2002JB001927.
Liivamägi, S., Somelar, P., Vircava, I., Mahaney, W.C., Kirs, J., Kirsimäe, K., 2015. Petrology, mineralogy and geochemical climofunctions of the Neoproterozoic Baltic paleosol. Precambrian Res. 256, 170–188.
Linol, B., de Wit, M.J., Guillocheau, F., de Wit, M.C.J., Anka, Z., Colin, J.P., 2015a. Formation and collapse of the Kalahari Duricrust ['African Surface'] across the Congo Basin, with implications for changes in rates of Cenozoic off-shore sedimentation. In: de Wit, M.J., Guillocheau, F., de Wit, M.J.C. (Eds.), Geology and Resource Potential of the Congo Basin, Regional Geology Reviews. Springer-Verlag, Berlin Heidelberg, pp. 193–210.
Linol, B., de Wit, M.J., Barton, E., Guillocheau, F., de Wit, M.J.C., Colin, J.P., de Wit, M.J., de Wit, M.J.C., 2015b. Paleogeography and tectono-stratigraphy of Carboniferous–Permian and Triassic 'Karoo-like' sequences of the Congo Basin. In: Guillocheau, F. (Ed.), Geology and Resource Potential of the Congo Basin, Regional Geology Reviews. Springer-Verlag, Berlin Heidelberg, pp. 111–134.
Linol, B., de Wit, M.J., Barton, E., Guillocheau, F., de Wit, M.J.C., Colin, J.P., de Wit, M.J., de Wit, M.J.C., 2015c. Facies analysis, chronostratigraphy, and paleo-environmental reconstructions of the Jurassic to Cretaceous sequences of the Congo Basin. In: Guillocheau, F. (Ed.), Geology and Resource Potential of the Congo Basin, Regional Geology Reviews. Springer-Verlag, Berlin Heidelberg, pp. 135–161.
Linol, B., de Wit, M.J., Guillocheau, F., Robin, C., Dauteuil, O., 2015d. Multiphase Phanerozoic subsidence and uplift history recorded in the Congo Basin – a complex successor basin. In: de Wit, M.J., Guillocheau, F., de Wit, M.J.C. (Eds.), Geology and Resource Potential of the Congo Basin, Regional Geology Reviews. Springer-Verlag, Berlin Heidelberg, pp. 213–227.
Linol, B., de Wit, M.J., Barton, E., de Wit, M.J.C., Guillocheau, F., 2016. U-Pb detrital zircon dates and source provenance analysis of Phanerozoic sequences of the Congo Basin, Central Gondwana. Gondwana Res. 29, 208–219.
Lucazeau, F., Brigaud, F., Leturmy, P., 2003. Dynamic interactions between the Gulf of Guinea passive margin and the Congo River drainage basin: 2. Isostasy and uplift. J. Geophys. Res. Solid Earth 108 (B8), 2384. https://doi.org/10.1029/2002JB001928.
Macdonald, F.A., Schmitz, M.D., Crowley, J.L., Roots, C.F., Jones, D.S., Maloof, A.C., Strauss, J.V., Cohen, P.A., Johnston, D.T., Schrag, D.P., 2010. Calibrating the Cryogenian. Science 327, 1241–1243.
Mann, M., 2005. The Dark Side of Democracy: Explaining Ethnic Cleansing. Cambridge University Press, Cambridge, pp. 580.
Masih, I., Maskey, S., Mussá, F.E.F., Trambauer, P., 2014. A review of droughts on the African continent: a geospatial and long-term perspective. Hydrol. Earth Syst. Sci. 18 (9), 3635–3649.
McBride, E.F., 1985. Diagenetic processes that affect provenance determinations in sandstones. In: Zuffa, G.G. (Ed.), Provenance of Arenites. NATO ASI Series, vol. 148. Reidel, Dordrecht, pp. 95–113.
McBride, E.F., Abel-Wahab, A., McGilvery, T.A., 1996. Loss of sand-size feldspar and rock fragments along the South Texas Barrier Island, USA. Sediment. Geol. 107, 37–44.
McCauley, R.N., 2011. Why Religion Is Natural and Science Is Not. Oxford University Press, Oxford (UK), pp. 352.
McDonough, W.F., Sun, S.S., 1995. The composition of the Earth. Chem. Geol. 120,

223–253.
McGinnis, J.P., Driscoll, N.W., Karner, G.D., Brumbaugh, W.D., Cameron, N., 1993. Flexural response of passive margins to deep-sea erosion and slope retreat: Implications for relative sea-level change. Geology 21 (10), 893–896.
Mehring, J.L., McBride, E.F., 2007. Origin of modern quartzarenite beach sands in a temperate climate, Florida and Alabama, USA. Sediment. Geol. 201, 432–445.
Muhs, D.R., 2004. Mineralogical maturity in dunefields of North America, Africa and Australia. Geomorphology 59, 247–269.
Négrel, P., Allègre, C.J., Dupré, B., Lewin, E., 1993. Erosion sources determined by inversion of major and trace element ratios and strontium isotopic ratios in river water: the Congo Basin case. Earth Planet. Sci. Lett. 120, 59–76.
Nesbitt, H.W., Young, G.M., 1982. Early Proterozoic climates and plate motions inferred from major element chemistry of lutites. Nature 299, 715–717.
Njome, M.S., de Wit, M.J., 2014. The Cameroon Line: analysis of an intraplate magmatic province transecting both oceanic and continental lithospheres: constraints, controversies and models. Earth Sci. Rev. 139, 168–194.
Norton, K., Schlunegger, F., 2011. Migrating deformation in the Central Andes from enhanced orographic rainfall. Nat. Commun. 2, 584. https://doi.org/10.1038/ncomms1590.
Oberg, K., Shelton, J.M., Gardiner, N., Jackson, P.R., 2009. Discharge and other hydraulic measurements for characterizing the hydraulics of lower Congo River, July 2008. In: Proceedings of the International Association for Hydraulic Research Congress. vol. 33. pp. 8.
Odom, I.E., Doe, T.W., Dott, R.H., 1976. Nature of feldspar-grain size relations in some quartz-rich sandstones. J. Sediment. Petrol. 46, 862–870.
Parker, A., 1970. An index of weathering for silicate rocks. Geol. Mag. 107, 501–504.
Pedrosa-Soares, A.C., Alkmim, F.F., Tack, L., Noce, C.M., Babinski, M., Silva, L.C., Martins-Neto, M.A., 2008. Similarities and differences between the Brazilian and African counterparts of the Neoproterozoic Araçuaí–West Congo orogen. In: Pankhurst, R.J., Trouw, R.A.J., Brito Neves, B.B., de Wit, M.J. (Eds.), West Gondwana: Pre-Cenozoic Correlations across the South Atlantic Region. vol. 294. pp. 153–172 Geological Society, London, Special Publications.
Peters, C.R., O'Brien, E.M., 2001. Palaeo-lake Congo: Implications for Africa's late Cenozoic climate—some unanswered questions. In: Heine, K., Runge, J. (Eds.), Palaeoecology of Africa and the Surrounding Islands. Proceedings of the 25th Inqua Conference, Durban, South Africa, 3–11 August 1999, vol. 27. CRC Press, Boca Raton (FL), pp. 11–18.
Petschick, R., Kuhn, G., Gingele, F., 1996. Clay mineral distribution in surface sediments of the South Atlantic: Sources, transport, and relation to oceanography. Mar. Geol. 130, 203–229.
Pettijohn, F.J., 1954. Classification of sandstones. J. Geol. 62, 360–365.
Pettijohn, F.J., Potter, P.E., Siever, R., 1972. Sand and Sandstone. Springer, New-York Heidelberg, pp. 618.
Popper, K., 1994. Historicism and the myth of destiny. In: The Open Society and its Enemies. Princeton University Press, Princeton, pp. 7–9.
Potter, P.E., Franzinelli, E., 1985. Fraction analyses of modern river sand of Rios Negro and Solimões, Brazil. Impllcations for the origin of quartz-rich sandstones. Rev. Bras. Geosci. 15, 31–35.
Prave, A.R., Condon, D.J., Hoffmann, K.H., Tapster, S., Fallick, A.E., 2016. Duration and nature of the end-Cryogenian (Marinoan) glaciation. Geology 44, 631–634.
Resentini, A., Andò, S., Garzanti, E., 2018. Quantifying roundness of detrital minerals by image analysis: Sediment transport, shape effects, and provenance implications. J. Sediment. Res. 88, 276–289.
Rieu, R., Allen, P.A., Plötze, M., Pettke, T., 2007. Compositional and mineralogical variations in a Neoproterozoic glacially influenced succession, Mirbat area, South Oman: Implications for paleoweathering conditions. Precambrian Res. 154, 248–265.
Roberts, E., Jelsma, H.A., Hegna, T., 2015. Mesozoic sedimentary cover sequences of the Congo Basin in the Kasai Region, Democratic Republic of Congo. In: de Wit, M.J., Guillocheau, F., de Wit, M.J.C. (Eds.), Geology and Resource Potential of the Congo Basin. Regional Geology Reviews Springer-Verlag, Berlin Heidelberg, pp. 163–191.
Rooney, A.D., Strauss, J.V., Brandon, A.D., Macdonald, F.A., 2015. A Cryogenian chronology: two long-lasting synchronous Neoproterozoic glaciations. Geology 43, 459–462.
Rudnick, R.L., Gao, S., 2003. Composition of the continental crust. In: Rudnick, R.L., Holland, H.D., Turekian, K.K. (Eds.), Treatise on Geochemistry. The Crust, vol. 3. Elsevier Pergamon, Oxford, pp. 1–64.
Runge, J., 2007. The Congo River, Central Africa. In: Gupta, A. (Ed.), Large Rivers: Geomorphology and Management. Wiley, New York, pp. 293–309.
Savoye, B., Cochonat, P., et al., 38 authors, 2000. Structure et évolution récente de l'éventail turbiditique du Zaïre: premiers résultats scientifiques des missions d'exploration Zaïango 1 & 2 (marge Congo–Angola). C. R. Acad. Sci. Ser. IIA-Earth Planet. Sci. 331 (3), 211–220.
Savoye, B., Babonneau, N., Dennielou, B., Bez, M., 2009. Geological overview of the Angola–Congo margin, the Congo deep-sea fan and its submarine valleys. Deep-Sea Res. II Top. Stud. Oceanogr. 56 (23), 2169–2182.
Schulz, M.S., White, A.F., 1999. Chemical weathering in a tropical watershed, Luquillo Mountains, Puerto Rico III: quartz dissolution rates. Geochim. Cosmochim. Acta 63, 337–350.
Schulz, H.D., Beese, D., Breitzke, M., Brück, L., Brügger, B., Dahmke, A., Dehning, K., Diekamp, V., Dünner, B., Ehrhardt, I., Gerlach, H., Giese, M., Glud, R., Gumprecht, R., Gundersen, J., Henning, R., Hinrichs, S., Petermann, H., Richter, M., Sagemann, J., Schmidt, W., Schneider, R., Scholz, M., Segl, M., Werner, U., Zabel, M., 1992. Bericht und erste Ergebnisse über die Meteor-Fahrt M20/2, Abidjan-Dakar, 27.12.1991-3.2.1992. In: Berichte aus dem Fachbereich Geowissenschaften der Universität Bremen, 025. vol. 25. Department of Geosciences, Bremen University, pp. 175.
Schwanghart, W., Scherler, D., 2014. TopoToolbox 2 – MATLAB-based software for topographic analysis and modeling in Earth surface sciences. Earth Surf. Dyn. 2, 1–7. https://doi.org/10.5194/esurf-2-1-2014.
Sciunnach, D., Garzanti, E., 1996. Sedimentary record of late Paleozoic rift and break-up in Northern Gondwana (Thini Chu Group and Tamba-Kurkur Fm.; Dolpo Tethys Himalaya, Nepal). Geodin. Acta 9, 41–56.
Séranne, M., Anka, Z., 2005. South Atlantic continental margins of Africa: a comparison of the tectonic vs climate interplay on the evolution of equatorial West Africa and SW Africa margins. J. Afr. Earth Sci. 43 (1–3), 283–300.
Shepard, F.P., Emery, K.O., 1973. Congo submarine canyon and fan valley. Am. Assoc. Pet. Geol. Bull. 57 (9), 1679–1691.
Showers, K.B., 2009. Congo River's Grand Inga hydroelectricity scheme: linking environmental history, policy and impact. Water Hist. 1, 31–58.
Sláma, J., Košler, J., Condon, D.J., Crowley, J.L., Gerdes, A., Hanchar, J.M., Horstwood, M.S., Morris, G.A., Nasdala, L., Norberg, N., Schaltegger, U., 2008. Plešovice zircon — a new natural reference material for U–Pb and Hf isotopic microanalysis. Chem. Geol. 249, 1–35.
Snyder, N., Whipple, K., Tucker, G., Merritts, D., 2000. Landscape response to tectonic forcing: Digital elevation model analysis of stream profiles in the Mendocino triple junction region, northern California. Geol. Soc. Am. Bull. 112, 1250–1263.
Spiess, V., Shipboard Party, 2012. Meteor Berichte 12–2, Cruise 76, Leg 3a, Walvis Bay—Walvis Bay, June 07–July 13, 2008. Insitiute of Oceanography, University of Hamburg, Hamburg, pp. 43.
Stankiewicz, J., de Wit, M.J., 2006. A proposed drainage evolution model for Central Africa—did the Congo flow east? J. Afr. Earth Sci. 44, 75–84.
Straathof, G.B., 2011. Neoproterozoic Low Latitude Glaciations: An African Perspective. Ph.D. Thesis. University of Edinburgh, pp. 285.
Stumm, W., Morgan, J.J., 1996. Aquatic Chemistry. John Wiley & Sons. Inc., New York (1022 p).
Suttner, L.J., Basu, A., Mack, G.H., 1981. Climate and the origin of quartz arenites. J. Sediment. Petrol. 51, 1235–1246.
Tack, L., 1973. Le massif de la Lufu et sa bordure (République du Zaïre). In: Note préliminaire. Annales de la Société géologique de Belgique, vol. 96. pp. 31–47.
Tack, L., 1975. Bijdrage tot de studie van de geologie. In: de Petrografie en de petrologie van het Mayumbiaan van Neder-Zaïre, Unpublished Ph.D. Thesis, Rijksuniversiteit Gent (Belgium), 200 p. + annexes.
Tack, L., 1979. Données pétrochimiques concernant les roches vertes de la région d'Inga au Bas-Zaïre. vol. 102. Annales de la Société Géologique de Belgique, pp. 181–183.
Tack, L., Wingate, M.T.D., Liégeois, J.P., Fernandez-Alonso, M., Deblond, A., 2001. Early Neoproterozoic magmatism (1000–910 Ma) of the Zadinian and Mayumbian groups (Bas-Congo): Onset of Rodinia rifting at the western edge of the Congo craton. Precambrian Res. 110, 277–306.
Tack, L., Delvaux, D., Kadima, E., Delpomdor, F., Tahon, A., Dumont, P., Hanon, M., Fernandez-Alonso, M., Baudet, D., Dewaele, S., Cibambula, E., Kanda Nkula, V., Mpiana, Ch., 2008. The 1.000 m thick redbeds sequence of the Congo River Basin (CRB): A generally overlooked testimony in Central Africa of post-Gondwana amalgamation (550 Ma) and pre-Karoo break-up (320 Ma). In: 22nd Colloquium African Geology (CAG22), November 04–06, 2008, Hammamet, Tunisia, pp. 86–88.
Tait, J., Delpomdor, F., Préat, A., Tack, L., Straathof, G., Nkula, V.K., 2011. Neoproterozoic sequences of the West Congo and Lindi/Ubangi Supergroups in the Congo Craton, Central Africa. In: Arnaud, E., Halverson, G.P., Shields-Zhou, G. (Eds.), The Geological Record of Neoproterozoic Glaciations, pp. 185–194 Geological Society, London, Memoir 36.
Taylor, S.R., McLennan, S.M., 1995. The geochemical evolution of the continental crust. Rev. Geophys. 33, 241–265.
Todd, T.W., 1968. Paleoclimatology and the relative stability of feldspar minerals under atmospheric conditions. J. Sediment. Petrol. 38, 832–844.
Uenzelmann-Neben, G., 1998. Neogene sedimentation history of the Congo Fan. Mar. Pet. Geol. 15, 635–650.
van der Gaast, S.J., Jansen, J.H.F., 1984. Mineralogy, opal, and manganese of middle and late Quaternary sediments of the Zaire (Congo) deep-sea fan: Origin and climatic variation. Neth. J. Sea Res. 17, 313–341.
van Loon, A.J., 2009. Unravelling the enigmas of the 'silver sands' in the Dutch/German/Belgian border area. Neth. J. Geosci. 88 (3), 133–145.
van Loon, A.T., Mange, M.A., 2007. 'In situ' dissolution of heavy minerals through extreme weathering, and the application of the surviving assemblages and their dissolution characteristics to correlation of Dutch and German silver sands. In: Mange, M.A., Wright, D.T. (Eds.), Heavy Minerals in Use. Developments in Sedimentology, vol. 58. Elsevier, Amsterdam, pp. 189–213.
Veatch, A.C., 1935. Evolution of the Congo Basin. Geological Society of America, Memoir 3. pp. 183.
Velbel, M.A., 1993. Constancy of silicate-mineral weathering-rate ratios between natural and experimental weathering: Implications for hydrologic control of differences in absolute rates. Chem. Geol. 105, 89–99.
Velbel, M.A., 1999. Bond strength and the relative weathering rates of simple orthosilicates. Am. J. Sci. 299, 679–696.
Velbel, M.A., 2007. Surface textures and dissolution processes of heavy minerals in the sedimentary cycle: Eexamples from pyroxenes and amphiboles. In: Mange, M.A., Wright, D.T. (Eds.), Heavy Minerals in Use. Developments in Sedimentology, vol. 58. Elsevier, Amsterdam, pp. 113–150.
Vermeesch, P., 2018a. IsoplotR: a free and open toolbox for geochronology. Geosci. Front. 9, 1479–1493.
Vermeesch, P., 2018b. Dissimilarity measures in detrital geochronology. Earth Sci. Rev. 178, 310–321.
Vermeesch, P., Resentini, A., Garzanti, E., 2016. An R package for statistical provenance analysis. Sediment. Geol. 336, 14–25.
von Eynatten, H., Pawlowsky-Glahn, V., Egozcue, J.J., 2002. Understanding perturbation

on the simplex: a simple method to better visualise and interpret compositional data in ternary diagrams. Math. Geol. 34, 249–257.
von Eynatten, H., Tolosana-Delgado, R., Karius, V., 2012. Sediment generation in modern glacial settings: grain-size and source-rock control on sediment composition. Sediment. Geol. 280, 80–92.
von Eynatten, H., Tolosana-Delgado, R., Karius, V., Bachmann, K., Caracciolo, L., 2016. Sediment generation in humid Mediterranean setting: grain-size and source-rock control on sediment geochemistry and mineralogy (Sila Massif, Calabria). Sediment. Geol. 336, 68–80.
Wefer, G., Bleil, U., Müller, P.J., Schulz, H.D., Berger, W.H., Brathauer, U., Brück, L., Dahmke, A., Dehning, K., Durate-Morais, M.L., Fürsich, F., Hinrichs, S., Klockgeter, K., Kölling, A., Kothe, C., Makaya, J.F., Oberhänsli, H., Oschmann, W., Posny, J., Rostek, F., Schmidt, H., Schneider, R.R., Segl, M., Sobiesiak, M., Soltwedel, T., Spieß, V., 1988. Bericht über die Meteor-Fahrt M6-6, Libreville - Las Palmas, 18.2.1988 - 23.3.1988. In: Berichte aus dem Fachbereich Geowissenschaften der Universität Bremen, 003. vol. 3. Department of Geosciences, Bremen University, pp. 97.
Wenau, S., Spiess, V., Pape, T., Fekete, N., 2015. Cold seeps at the salt front in the lower Congo Basin II: the impact of spatial and temporal evolution of salt-tectonics on hydrocarbon seepage. Mar. Pet. Geol. 67, 880–893.
Whipple, K.X., 2004. Bedrock rivers and the geomorphology of active orogens. Annu. Rev. Earth Planet. Sci. 32, 151–185.
Wobus, C.W., Whipple, K.X., Kirby, E., Snyder, N., Johnson, J., Spyropolou, K., Crosby, B., Sheehan, D., 2006. Tectonics from topography: Procedures, promise, and pitfalls. Geol. Soc. Am. Spec. Pap., vol. 398, 55–74.
Woodhead, J.A., Rossman, G.R., Silver, N.T., 1991. The metamictization of zircon: Radiation dose-dependent structural characteristics. Am. Mineral. 76, 74–82.